Structures of *Staphylococcus aureus* Cell-Wall Complexes with Vancomycin, Eremomycin, and Chloroeremomycin Derivatives by $^{13}C\{^{19}F\}$ and $^{15}N\{^{19}F\}$ Rotational-Echo Double Resonance†

Sung Joon Kim,‡,§ Lynette Cegelski,§ Maria Preobrazhenskaya,|| and Jacob Schaefer*,§

Department of Molecular Biophysics, Washington University School of Medicine, St. Louis, Missouri 63110, Department of Chemistry, Washington University, St. Louis, Missouri 63130, and Gause Institute of New Antibiotics, Russian Academy of Medical Sciences, Moscow 119021, Russia

Received December 30, 2005; Revised Manuscript Received February 20, 2006

ABSTRACT: Solid-state NMR has been used to examine isolated cell walls and intact whole cells of *Staphylococcus aureus* complexed to five different vancomycin, eremomycin, and chloroeremomycin derivatives. The cell walls and whole cells were specifically labeled with D-[1-^{13}C]alanine, or a combination of [1-^{13}C]glycine and [ϵ-^{15}N]lysine. Each of the bound glycopeptides had a ^{19}F-labeled substituent at either its *C*-terminus or its disaccharide position. The $^{13}C\{^{19}F\}$ rotational-echo double-resonance (REDOR) dephasing for the cell-wall ^{13}C-labeled bridging pentaglycyl segment connecting a glycopeptide-complexed peptidoglycan stem with its neighboring stem indicates that the fluorine labels for all bound glycopeptides are positioned at one or the other end of the bridge. An exception is *N*′-(*p*-trifluoromethoxybenzyl)-chloroeremomycin, whose hydrophobic substituent differs in length by one phenyl group compared to that of oritavancin, *N*′-4-[(4-chlorophenyl)benzyl)]chloroeremomycin. For this drug, the fluorine label is near the middle of the pentaglycyl segment. $^{15}N\{^{19}F\}$ REDOR dephasing shows the proximity of the fluorine to the bridge-link site of the pentaglycyl bridge for *C*-terminus-substituted moieties and the cross-link site for disaccharide-substituted moieties. Full-echo REDOR spectra of cell-wall complexes from cells labeled by D-[1-^{13}C]alanine (in the presence of an alanine racemase inhibitor) reveal three different carbonyl carbon chemical-shift environments, arising from the D-Ala-D-Ala binding site and the D-Ala-Gly-1 cross-link site. The REDOR results indicate a single fluorine dephasing center in each peptidoglycan complex. Molecular models of the mature cell-wall complexes that are consistent with internuclear distances obtained from $^{13}C\{^{19}F\}$ and $^{15}N\{^{19}F\}$ REDOR dephasing allow a correlation of structure and antimicrobial activity of the glycopeptides.

Vancomycin is a potent antibiotic that is effective against multi-drug-resistant Gram-positive bacteria including methicillin-resistant *S. aureus*. As many as 60% of clinically isolated strains of *S. aureus* are methicillin resistant (*1*), which means that vancomycin is one of the most important antibiotics in use today. Vancomycin inhibits the transglycosylation step in the peptidoglycan biosynthesis of cell walls (*2*, *3*) by binding to the D-Ala-D-Ala carboxyl termini of pentapeptide stems of nascent (immature) peptidoglycan (Figure 1) and peptidoglycan pentapeptide precursors, including lipid II (*2*, *4*).

The emergence of vancomycin-resistant enterococci (VRE[1]) has limited vancomycin usage against methicillin-resistant *S. aureus*. In 2002, vancomycin-resistant *S. aureus* (VRSA) with a minimum inhibitory concentration (MIC) of greater than 128 μg/mL was recovered from a patient in Michigan who was being treated with multiple antibiotics (*5*). *E. faecalis*, a vancomycin-resistant enterococcus, was also recovered from the patient. The VRSA isolate contained the *vanA* vancomycin-resistance gene, probably through conjugative transfer from the VRE isolate (*6*). The *vanA* gene codes for the pentapeptide-stem D-Ala-D-Lac terminus, which results in reduced vancomycin binding (*7*, *8*). Obviously, new glycopeptides are needed to combat these virulent bacterial strains.

Fluorophenylbenzyl-vancomycin (FPBV) is a vancomycin derivative exhibiting improved activity against VRE that have D-Ala-D-Lac stem termini. FPBV is an analogue of [^{19}F]-

† This paper is supported by the National Institutes of Health Grant EB02058.

* To whom correspondence should be addressed. Tel: 314-935-6844. Fax: 314-935-4481. E-mail: jschaefer@wustl.edu.

‡ Department of Molecular Biophysics, Washington University School of Medicine.

§ Department of Chemistry, Washington University.

|| Russian Academy of Medical Sciences.

[1] Abbreviations: CPBV, *N*′-[*p*-(*p*-chlorophenyl)benzyl]vancomycin; CPMAS, cross-polarization magic-angle spinning; FPBV, 4-(4-fluorophenyl)benzylvancomycin; GISA, glycopeptide-intermediate *S. aureus*; GRE, glycopeptide-resistant enterococci; GSE, glycopeptide-susceptible enterococci; HBPyU, (benzotriazol-1-yloxy)dipyrrolidinocarbenium hexafluorophosphate; LCTA-1049, eremomycin *p*-fluorobenzylamide; LCTA-1110, eremomycin *p*-fluorophenylpiperazinamide; lipid II, *N*-acetylglucosamine-*N*-acetyl-muramyl-pentapeptide-pyrophosphoryl-undecaprenol; LY329332, *N*′-4-[(4-fluorophenyl)-benzyl)]chloroeremomycin; LY309687, *N*′-(*p*-trifluoromethoxybenzyl)-chloroeremomycin; MD, molecular dynamics; MIC, minimum inhibitory concentration; PG, peptidoglycan; PyBOP, (benzotriazole-1-yloxy)-tripyrrolidinophosphonium hexafluorophosphate; REDOR, rotational-echo double resonance; ssb, spinning sideband; TEDOR, transferred-echo double resonance; VRE, vancomycin-resistant enterococci; VSE, vancomycin-susceptible enterococci.

10.1021/bi052660s CCC: $33.50
Published on Web 03/30/2006

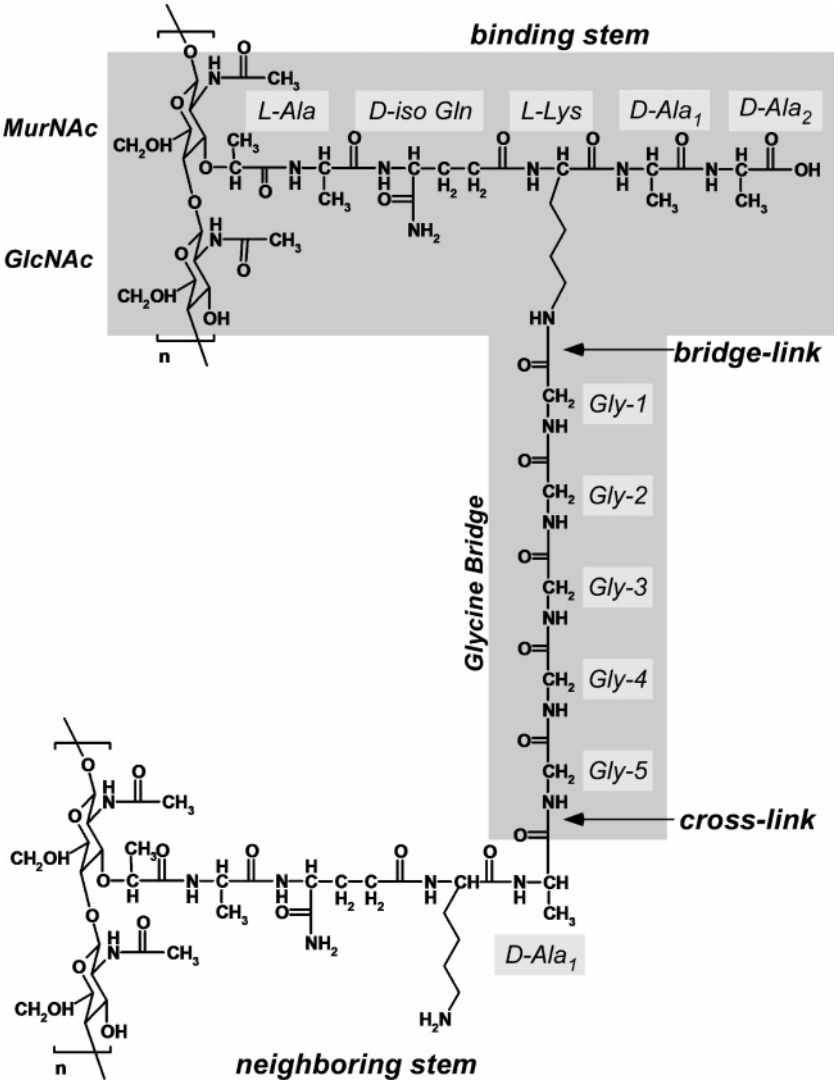

FIGURE 1: Chemical structure of the peptidoglycan of *S. aureus.* The highlighted portion shows the components of a single repeat unit of the cell-wall peptidoglycan polymer.

oritavancin (Eli Lilly, compound LY329332), a chloroeremomycin derivative (*9*). Both have a hydrophobic fluorophenylbenzyl disaccharide substituent, and both show 100-fold increased activity, relative to their parent compounds (Figure 2, vertical arrows) on standard tests against VRE (*10*−*13*). In addition, the 4-epi-vancosamine attached to the sixth amino acid backbone position of chloroeremomycin and [^{19}F]oritavancin increases the antimicrobial activity against VRE by 10-fold, relative to their nonsubstituted analogues, vancomycin and FPBV, respectively (Figure 2, horizontal arrows). Thus, both disaccharide substitution and the presence or absence of 4-epi-vancosamine appear to be important factors for the enhanced antimicrobial activity of these vancomycin-like glycopeptides.

The length of the hydrophobic disaccharide moiety also affects antimicrobial activity. For example, reaction of the amine-sugar of chloroeremomycin with trifluoromethoxybenzaldehyde produces the glycopeptide antibiotic LY309687, which is only 10-fold more potent than chloroeremomycin in an in vitro VRE assay (Figure 3). Thus, the relatively short length of its fluorinated side chain reduces potency by a factor of 10 relative to that of [^{19}F]oritavancin, despite the presence of the 4-epi-vancosamine substituent.

In addition to size, the position of the hydrophobic moiety affects the activity of glycopeptides. The LCTA eremomycin derivatives shown in Figure 4 have substituent chain lengths that are similar to those of LY309687 and [^{19}F]oritavancin, but these moieties are located at the *C*-terminus of an eremomycin core, instead of at the disaccharide position. The LCTA compounds have reduced potency (relative to their parent compounds) against vancomycin-susceptible strains but modestly improved potency against vancomycin-resistant strains (Table 1).

In this article, we report the results of rotational-echo double-resonance (*14*) (REDOR) NMR studies of FPBV, LY309687, LCTA-1049, and LCTA-1110 bound to cell walls and whole cells of *S. aureus*. The experiments were similar to those performed earlier on [^{19}F]oritavancin−PG complexes (*15*). REDOR was used to measure the dipolar couplings between ^{19}F of the drugs and ^{13}C and ^{15}N labels incorporated in peptidoglycan (PG) stems and bridging pentaglycyl segments. Because of its large magnetic moment, the ^{19}F probe allows the measurement of C−F distances of up to 12 Å (*15*) and N−F distances of 8 Å (*15*). The ^{13}C−^{19}F and ^{15}N−^{19}F distances from the REDOR experiments were then used to build model structures for all five glycopeptide−PG

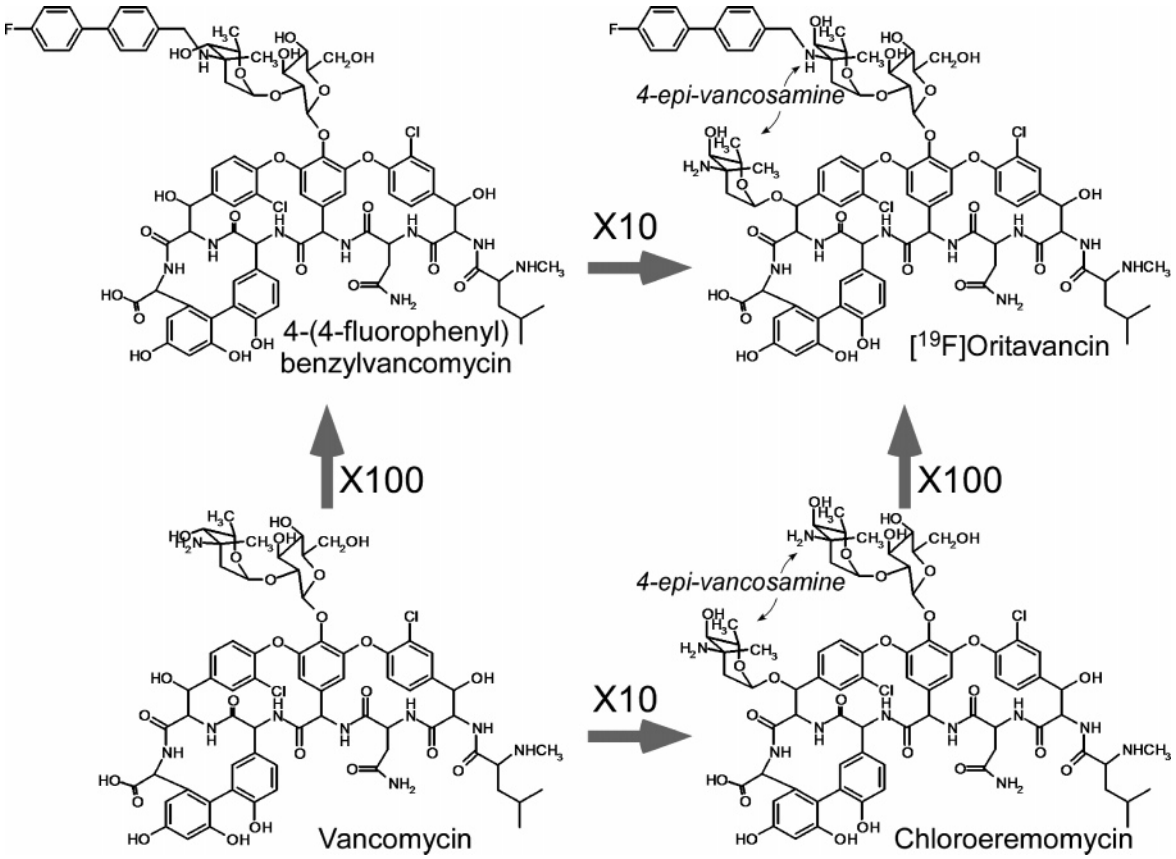

FIGURE 2: Structures of vancomycin, chloroeremomycin, and two of their analogues. The arrows show the relative enhancements of glycopeptide antimicrobial activities against VRE.

complexes. The possible roles played by the disaccharide substituent and the 4-epi-vancosamine moiety in enhancing glycopeptide potency against VRE are inferred from the comparisons of the models (all of which are variations on a single theme) and the antimicrobial activities of the drugs. These comparisons lead to a suggestion for the mode of action of this class of glycopeptide antibiotic and a rationale for the correlation of the mode of action with the structures of mature glycopeptide−peptidoglycan complexes.

MATERIALS AND METHODS

Synthesis of 4-Fluorophenyl-benzaldehyde and 4-(4-Fluorophenyl)benzylvancomycin. 4-Fluorophenyl-benzaldehyde was synthesized using palladium to catalyze the Suzuki cross-coupling reaction of 4-fluorophenyl-boronic acid and 4-bromobenzaldehyde (*16*). FPBV was synthesized by reaction of the vancosamine sugar amine with 4-fluorophenyl-benzaldehyde, as described by Nagarajan et al. (*17*). Briefly, to 50 mg (33 μmol) of vancomycin dissolved in 1 mL of water were added 12 mL of 50:50 v/v MeOH/DMF and 3 mg of 4-fluorobenzaldehyde (24 μmol). The mixture was stirred under N_2 gas at room temperature. After 2 h, 10 mg of $NaBH_3CN$ was added to the reaction mixture. The reaction ran for 2 days, and the progress was monitored by HPLC. The final product, FPBV, has a retention time of 4.9 min on a C18 column, Zorbax SB-Aq (Agilent Technologies, Palo Alto, CA) 4.6 mm ID × 50 mm (100 Å particle size), with a flow rate of 1 mL/min. FPBV was purified from the reaction mixture using a semipreparative C18 column, Microsorb C18 (Varian, Palo Alto, CA) 21.4 ID × 250 mm (100 Å particle size), at a flow rate of 10 mL/min. The fraction containing FPBV was concentrated using a rotary evaporator. The final pH was adjusted to 3.2. Lyophilization yielded 20 mg of white powder. The MS-MALDI calculated mass for FPBV, $C_{79}H_{84}Cl_2FN_9O_{24}$, [M + Na^+] was 1656.5, and the found mass was 1656.7.

Synthesis of LCTA-1049 and LCTA-1110. Carboxamides LCTA-1049 and LCTA-1110 were obtained by the condensation of eremomycin with hydrochlorides of 4-fluorobenzylamine or 4-fluorophenylpiperazine using PyBOP or HBPyU as condensing reagents with yields of about 80%, as described earlier (*18*). The MS-ESI calculated mass for LCTA-1049, $C_{80}H_{95}N_{11}O_{25}ClF$, [M + H^+] was 1664.6, and the found mass was 1664.5. The MS-ESI calculated mass for LCTA-1110, $C_{80}H_{100}N_{12}O_{25}ClF$, [M + H^+] was 1719.5, and the found mass was 1719.5.

Susceptibility Testing. Minimum inhibitory concentrations (MICs) were determined by the microdilution method using Mueller−Hinton broth as recommended by the National Committee for Clinical Laboratory Standards procedure as previously described (*19*).

Growth of Cells and the Formation of Complexes. S. aureus cells were grown on 300 mL of defined media (*20*) containing [1-^{13}C]glycine and L-[ϵ-^{15}N]lysine. The cells were harvested at OD_{660} = 1.0 and were complexed with 6.7 mg (4.0 μmol) of FPBV, resulting in 66% cell-wall binding-site occupancy (*15*). A second sample contained 6.7 mg of LY309687 (3.7 μmol) complexed with whole cells for 60% binding-site occupancy. The third and fourth samples each contained 4.9 mg of LCTA-1049 (2.9 μmol) and 4.9 mg of LCTA-1110 (2.8 μmol) complexed with whole cells grown on 500 mL of defined media for 30% and 29% binding-site

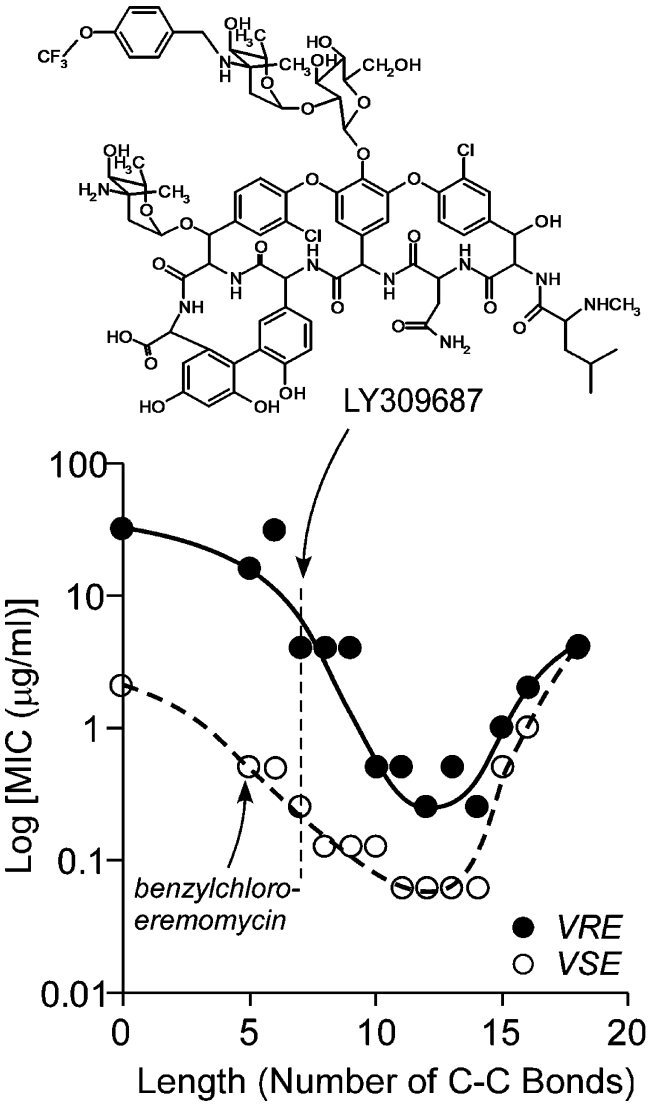

FIGURE 3: Minimum inhibitory concentrations of chemically modified chloroeremomycins against VRE (*E. faecium* VanA type, ●) and VSE (*E. faecium*, ○). The MICs are plotted as a function of the length (number of carbon−carbon bonds) of the side chain attached to the vancosamine of the disaccharide substituent (taken from Allen et al.) (*39*). The C−C bond side chain length of 0 corresponds to the parent compound chloroeremomycin, 5 to benzylchloroeremomycin, 6 to 4-hydroxybenzylchloroeremomycin, and 7 to 4-methoxybenzylchloroeremomycin. Those greater than 7 correspond to a series of *p*-alkoxybenzylchloroeremomycins with increasing aliphatic chain lengths. The structure of LY309687 is shown at the top of the figure.

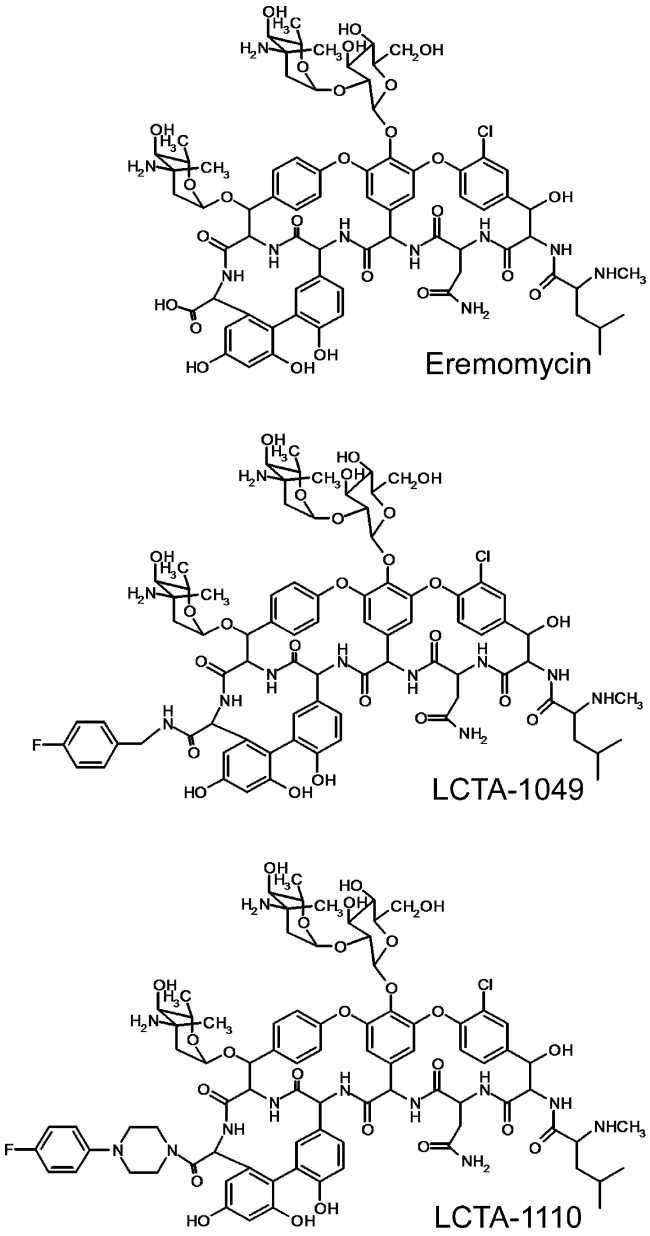

FIGURE 4: Structures of two LCTA glycopeptides and their parent compound, eremomycin.

occupancies, respectively. *S. aureus* cells were also grown on media containing D-[1-^{13}C]alanine, L-alanine and alaphosphin (5 μg/mL), an alanine racemase inhibitor. Both D- and L-alanine were needed for cell growth. Isolated D-[1-^{13}C]alanine-labeled cell walls (35.2 mg) were complexed with 6.6 mg of LY309687 (3.7 μmol) for 35% occupancy of cell-wall binding sites.

Rotational-Echo Double Resonance. The REDOR experiments were done in two parts: once with rotor-synchronized dephasing pulses (dephased echo, S) and once without (full echo, S_0). The dephasing pulses change the sign of the heteronuclear dipolar coupling, and this interferes with the spatial averaging resulting from the motion of the rotor during magic-angle spinning (*14*). The difference in signal intensity (REDOR difference, $\Delta S = S_0 - S$) for the observed spin (^{13}C or ^{15}N) in the two parts of the REDOR experiment is directly related to the corresponding distance to the dephasing spin (^{19}F).

REDOR was performed using a transmission-line probe (*21*) with a 17-mm long, 8.6-mm inside-diameter analytical coil and a Chemagnetics/Varian ceramic stator (Fort Collins, CO/Palo Alto, CA). The fluorine radio frequency (188 MHz) was coupled to the transmission line at an impedance minimum for the proton radio frequency (200 MHz). This provided about a 40 dB isolation between the tune-and-match circuits for each of the two frequencies (*21*) in addition to the isolation achieved by conventional filters and traps. The next lowest radio frequency in the cascade was carbon (50.3 MHz), which was introduced at a fluorine impedance minimum, and then nitrogen (20.3 MHz) at a carbon impedance minimum. In total, the single solonoidal coil of the probe was simultaneously tuned to four radiofrequencies, all of which were mutually isolated by the positions of their tuning circuits along the transmission line. The isolation eliminated

Table 1: Minimum Inhibitory Concentrations (μg/mL) of Vancomycin, Eremomycin, and *C*-terminus-Modified Eremomycins against Sensitive and Resistant Strains

compound/ strain	533 *S. epidermidis*	602 *S. haemolyticus*	3797 *S. aureus* (GISA)	3798 *S. aureus* (GISA)	568 *E. faecium* (GSE)	559 *E. faecalis* (GSE)	569 *E. faecium* (GRE)	560 *E. faecalis* (GRE)
vancomycin	1	2	16	8	2	1	>128	>128
eremomycin	0.13	0.13	4	4	0.13	0.13	>128	>128
LCTA-1049	0.25	0.5	1	1	0.13	0.13	32	32
LCTA-1110	0.5	1	1	1	0.5	0.5	32	32

the detectable leakage (pulse artifacts) between channels.

Lyophilized cell-wall and whole-cell samples were contained in Chemagnetics/Varian 7.5-mm outside-diameter zirconia rotors. The rotors were spun at 5000 Hz with the speed under active control to within ±2 Hz. A Tecmag (Houston, TX) pulse programmer controlled the spectrometer.

The radio frequency pulses for ^{13}C and ^{15}N were produced by 1-kW ENI (Andover, MA) LPI-10 power amplifiers. The radio frequency pulses for ^{1}H were produced by a 1-kW Kalmus Engineering Int., Ltd. (Valencia, CA) power amplifier, and the ^{19}F pulses by a 1-kW Dressler Hochfrequenztechnik Gmbh (Stolberg-Vicht, Germany) power amplifier. All four amplifiers were under active control. After the completion of data acquisition for each S or S_0 REDOR scan and before the re-cycle delay period, which was 2 s for these experiments, each amplifier in turn produced a 300-μs test pulse with the pulses separated from one another by 100 μs. The resulting voltage was capacitively sampled from a position along the transmission line (out of the magnetic field), where the voltage is proportional to that at the coil, diode detected, and compared to a reference voltage that had been previously calibrated by an NMR signal from a standard sample. The resulting difference voltage (typically 1 part in 500) was used to correct the drive of the final-stage power amplifier for the next repetition of the REDOR pulse sequence. This active control eliminated long-term drifts in the performance of the spectrometer due to component aging and minor changes in the temperature of the room, spinning gas, and power amplifiers. The S and S_0 alternate-scan strategy compensated for the short-term drifts. Thus, improvements in the sensitivity of S/S_0 and $\Delta S/S_0$ ratios by data accumulation times of days to weeks were practical.

The π-pulse lengths were 10 μs for ^{19}F, ^{13}C, and ^{15}N. Standard XY-8 phase cycling (*22*) was used for all refocusing and dephasing pulses. This scheme effectively compensates for finite-pulse imperfections. When used with the transmission-line probe described above and a 7.5-mm ceramic rotor spinning at 5 kHz, 112-T_r $^{13}C\{^{15}N\}$ REDOR on a ^{13}C-^{15}N double-labeled emerimicin 1-9 benzyl ester analytical standard determined a $^{13}C-^{15}N$ distance of 4.2 ± 0.1 Å (*23*), in agreement with the X-ray analysis of 4.16 Å. The same XY-8 phase cycling resulted in experimental $^{13}C\{^{19}F\}$ dephasing that was within 4% of the theoretical dephasing for an analytical standard after 15 ms of dipolar evolution (*24*). An 89-mm bore Oxford (Cambridge, England) superconducting solenoid provided a 4.7-T static magnetic field. Proton-carbon matched cross-polarization transfers were made in 2 ms at 50 kHz. The single-frequency proton dipolar decoupling was 98 kHz throughout dipolar evolution and data acquisition.

Calculated REDOR Dephasing. Dephasing was calculated using the modified Bessel function expressions given by Mueller et al. (*25*) and de la Caillerie and Fretigny (*26*) for a spin-$^1/_2$ pair. The REDOR dephasing function for CF_3 was approximated by treating the three fluorines as a single super spin (with two spin quantum numbers, $I = 1/2$ and 3/2) placed at the center of the plane defined by the positions of the three fluorines. This approximation is valid for C−F distances of 6 Å or more and N−F distances of 5 Å or more (*27*). The abbreviation $^{19}F_3$ will be used to denote this super spin. The REDOR dephasing function of the methyl fluorines was a sum of two dephasing functions. The $I = 3/2$ function represents all three spins either parallel or antiparallel to the static magnetic field (↑↑↑ or ↓↓↓). The $I = 1/2$ function is derived when one of the spins is antiparallel, relative to the other spins: (↑↑↓), (↑↓↑), (↓↑↑), (↓↓↑), (↓↑↓), and (↑↓↓). Each dephasing function was weighted by the degeneracy of its eigenstate. The REDOR dephasing function for the methyl fluorines was summed over a Gaussian distribution of dipolar couplings corresponding to a distribution of isolated $^{13}C-^{19}F_3$ pairs. The distribution parameters (mean and width) were allowed to vary to minimize the root-mean-square deviation (RMSD) between the experimental and calculated dephasing (*28*). For the dephasing calculation of the bridge labeled by [1-^{13}C]glycine, a five glycyl α-helix was assembled and energy minimized using Insight II (MSI, San Diego, CA). The grid position of a single $^{19}F_3$ label relative to the pentaglycyl helix was varied, and the RMSD was minimized between experimental and calculated dephasing.

Molecular Modeling. A model peptidoglycan fragment was constructed by adding an energy-minimized pentaglycyl helix to the lysyl side chain of a stem fragment, L-Ala-D-iso-Gln-L-Lys-D-Ala-D-Ala, bound to [^{19}F]oritavancin. The core of the glycopeptide−peptidoglycan complex was an energy-minimized structure based on the crystal structure of chloroeremomycin bound to Lys-D-Ala-D-Ala (*29*). The pentaglycyl helix was positioned to satisfy REDOR restraints (*15*). The fluorine of [^{19}F]oritavancin was placed 5 Å from the closest [1-^{13}C]Gly at the cross-link end of the bridging pentaglycyl segment and 11 Å from the farthest [1-^{13}C]Gly at the bridge-link. The $^{13}C-^{19}F$ internuclear distance between ^{19}F of LY329332 to D-[1-^{13}C]Ala (cross-link to adjacent stem) was fixed at 8 Å. The resulting structure is similar to that of the full energy-minimized [^{19}F]oritavancin−PG complex reported by Cegelski et al. (*30*) and was the starting point for modeling peptidoglycan complexes with FPBV and LY309687 using DS ViewerPro (Accelrys, Inc.). The structures of the aglycon (binding pocket) and the D-Ala-D-Ala terminus of the bound peptidoglycan fragment, $(Gly)_5$-L-Ala-D-iso-Gln-Lys-D-Ala-D-Ala, were subsequently unaltered. The disaccharide (glucose and vancosamine) conformations

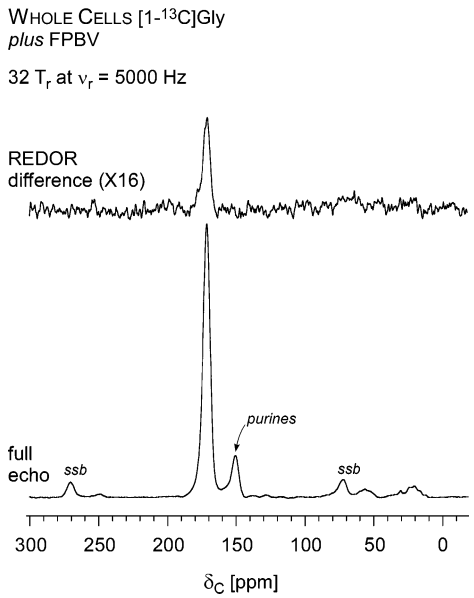

FIGURE 5: $^{13}C\{^{19}F\}$ REDOR spectra of whole cells of *S. aureus* labeled with [1-^{13}C]glycine and complexed with FPBV. The full-echo spectrum (S_0) is at the bottom of the figure, and the REDOR difference ($\Delta S = S_0 - S$, where S is the dephased echo) is shown at the top. The carbonyl carbons of the pentaglycyl bridges appear close to 170 ppm. The spectra are the result of the accumulation of 80 000 scans.

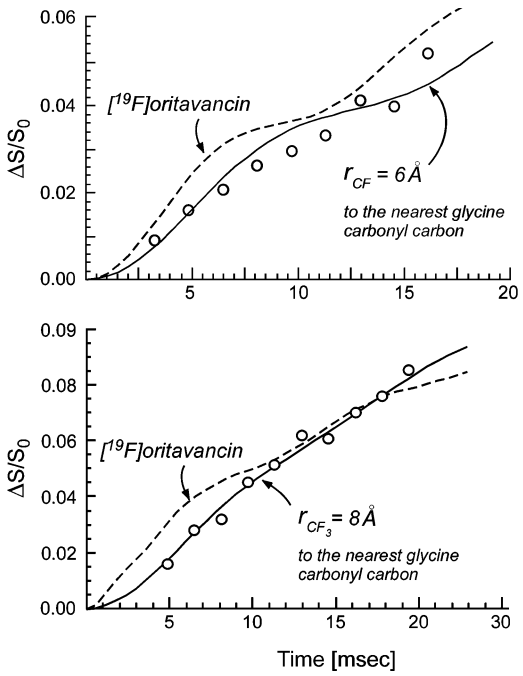

FIGURE 6: $^{13}C\{^{19}F\}$ dephasing ($\Delta S/S_0$) for whole cells of *S. aureus* labeled with [1-^{13}C]glycine and complexed with FPBV (top) and LY309687 (bottom). The solid lines are the calculated dephasing assuming the corresponding five $^{13}C-^{19}F$ distances in Figure 7 and a total dephasing of 12%. The dashed lines show the calculated dephasing assuming the five $^{13}C-^{19}F$ distances of the [^{19}F]-oritavancin−PG model in ref *15*. The dotted line in the bottom panel has been scaled so that the calculated dephasing matches the experimental dephasing near 15 ms.

were adjusted by rotations about the glycosidic bonds to position the ^{19}F and $^{19}F_3$ to satisfy all $^{13}C\{^{19}F\}$ REDOR distance constraints for the bridging pentaglycyl segment. The position of the *N*-terminus of the binding stem was varied to satisfy distances determined by $^{13}C\{^{19}F\}$ and $^{15}N\{^{19}F\}$ REDOR to bridge-link and cross-link sites.

RESULTS

FPBV Complex with [1-^{13}C]Gly-Labeled Whole Cells. The $^{13}C\{^{19}F\}$ REDOR NMR spectra of FPBV complexed with whole cells, grown on media containing [1-^{13}C]glycine and L-[ϵ-^{15}N]lysine after 6.4 ms of dipolar evolution are shown in Figure 5. Natural-abundance ^{13}C peptidoglycan peaks appear between 20 and 60 ppm in the full-echo spectrum (Figure 5, bottom). Some of the [1-^{13}C]glycine was used for the biosynthesis of purines (149 ppm). The full-echo carbonyl carbon peak at 171 ppm arises from glycyl residues in cell-wall pentaglycyl segments and all other proteins including those in the cytoplasm. The fraction of the peak due to cell-wall glycyls is 50%, as determined by an eight-rotor cycle $^{13}C\{^{15}N\}$ $\Delta S/S_0$ value of 0.1 (*3*). In that experiment, only the glycyl carbonyl-^{13}C covalently bonded to the ϵ-^{15}N (95% isotopic enrichment) of lysine at the bridge-link gives rise to dephasing, which means that the whole bridge is responsible for 5 times 0.1 or 50% of S_0.

The REDOR dephasing ($\Delta S/S_0$) as a function of dipolar evolution time for the complex of FPBV with *S. aureus* is shown in Figure 6 (top, open circles). The calculated dephasing is from five independent $^{13}C-^{19}F$ pairs (*15*). The weak $^{13}C-^{13}C$ coupling between carbonyl carbons of the pentaglycyl bridging segment is totally suppressed by fast magic-angle spinning, and the 3-bond J coupling is less than 10 Hz. The solid line is the calculated dephasing assuming the location of ^{19}F relative to the pentaglycyl bridge shown in Figure 7 (top) and a total dephasing of 12%. This arrangement provided the best match between calculated and observed dephasing and placed the ^{19}F at one end or the other of the pentaglycyl helix, 6 Å from the nearest glycyl carbonyl carbon and 11 Å from the farthest one. The corresponding C−F distances to the nearest and farthest glycyl carbonyl carbons in the [^{19}F]oritavancin−PG complex are 5 and 11 Å, respectively (*15*). The $^{13}C\{^{19}F\}$ dephasing calculated using the fluorine position in the [^{19}F]oritavancin complex is shown in Figure 6 as a dashed line. (The relative positions of the fluorine label for all of the complexes will be illustrated later.) The shapes of the solid and dashed lines are the same, just displaced from one another.

The asymptotic dephasing limit that was used for the fitting of the FPBV−PG dephasing in Figure 6 is 12%, reached after 35 ms of dipolar evolution. This limit can be calculated from the amount of complexed drug, known from the binding assay (*15*), and the fraction of cross-linked stems in the cell walls of *S. aureus*, directly determined by a transferred-echo double-resonance (TEDOR) experiment (*30*). Each pentaglycyl bridge is attached at its Gly-5 *C*-terminus to a stem by a lysyl ϵ-nitrogen; there are no pentaglycyl segments open at their *C*-termini. This stem may end in either D-Ala or D-Ala-D-Ala. Only the latter is a potential binding site. The TEDOR results of Cegelski et al. (*30*) indicate that 54% of stems end in D-Ala and 46% in D-Ala-D-Ala in mature cell walls. We assume no bias in the distribution of D-Ala-D-Ala stem ends and take 46% as the percentage of stems that are potential binding sites. We also assume that the fraction of pentaglycyl segments in lipid II within the cytoplasm is small and can be ignored compared to the fraction in the mature cell wall.

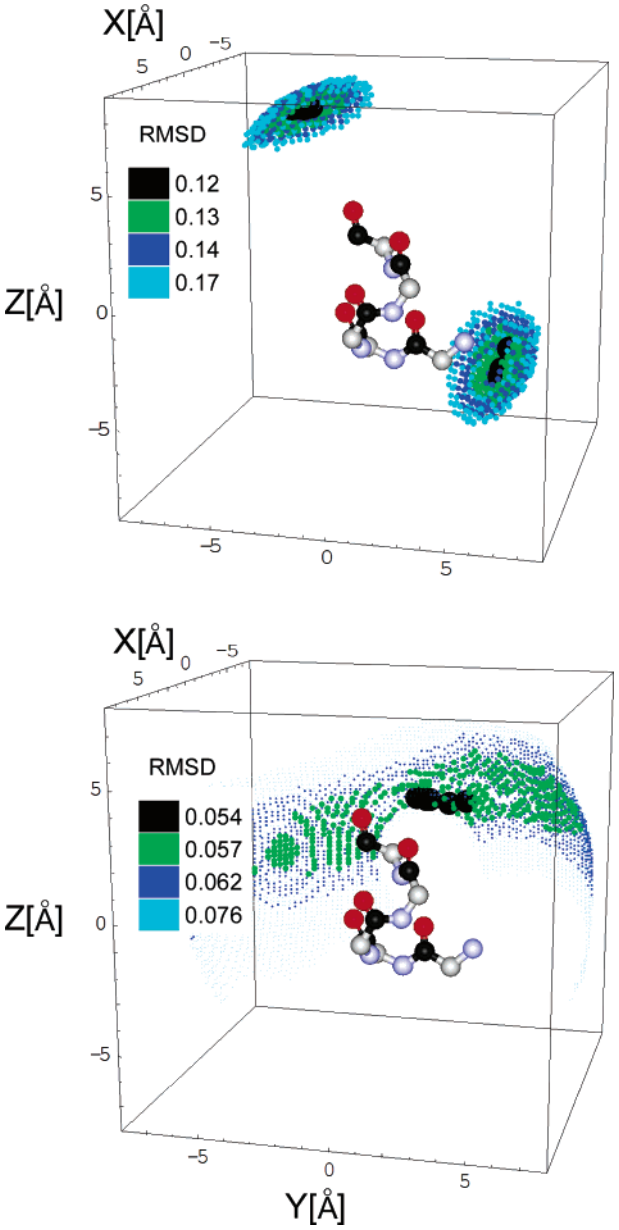

FIGURE 7: Possible positions of fluorine relative to the bridging pentaglycyl helix in peptidoglycan complexes of FPBV (top) and LY309687 (bottom). The positions that are consistent with the ^{13}C-$\{^{19}F\}$ dephasing of the carbonyl carbon signals of the bridge (carbonyl carbons in black, alpha carbons in gray, nitrogens in blue, and oxygens in red) are indicated by small dots whose colors indicate the root-mean-square deviation between calculated and experimental dephasing. The best match for FPBV places the fluorine along the helix axis, whereas that for LY309687 has the fluorine off of the axis and closer to the middle of the helix.

A binding assay (*15*) showed that two-thirds of all binding sites are occupied by FPBV. Thus, the fraction of all pentaglycyl segments that are near a fluorine in the FPBV−PG complex is (2/3)(0.46) = 31%, which is the calculated dephasing limit. Only half of the whole-cell S_0 is due to bridge glycyls (see above); therefore, the experimental value of about 12% should be multiplied by two to give a pentaglycyl segment $\Delta S/S_0$ observed dephasing limit of 24%. The fact that the observed limit is lower than the calculated value of 31% suggests that some pentaglycyl segments have an atypical conformation, possibly because they are not cross-linked at their Gly-1 *N*-terminus but are open (*15*). For these pentaglycyl segments, the local conformation could move some $^{13}C-^{19}F$ distances outside the limits of detectability for 30 ms of dipolar evolution.

LY309687 Complex with [1-^{13}C]Gly-Labeled Whole Cells. The $^{13}C\{^{19}F\}$ REDOR dephasing for LY309687 complexed with whole cells of *S. aureus* grown on media containing [1-^{13}C]glycine and L-[ϵ-^{15}N]lysine is shown in Figure 6 (bottom, open circles). The dephasing cannot be fit using a fluorine location similar to those of FPBV and [^{19}F]-oritavancin. The calculated dephasing in that situation (dashed line) can be made to match the experimental dephasing either between 5 and 10 ms of dipolar evolution or between 10 and 15 ms but not both. The best match occurs by moving the CF_3 of LY309687 away from one end or the other of the glycyl bridge and placing it closer to the middle (Figure 7, bottom). The nearest glycyl carbonyl carbon is then about 8 Å from the $^{19}F_3$ of LY309687, and the farthest one is 10 Å away. The $^{19}F_3$ super-spin position is still at least 10 Å away from the amide nitrogen connecting the bridge to the stem. The substantial difference between the allowed $^{19}F_3$ position of LY309687 and the ^{19}F position of the [^{19}F]oritavancin indicates a major conformational difference between these two structurally similar glycopeptides when they are bound to peptidoglycan.

The calculated asymptotic dephasing limit for the LY309687−PG complex is (0.60)(0.46) = 28%, where the first factor is the binding-site occupancy from the binding assay, and the second factor is the fraction of stems ending in D-Ala-D-Ala. The calculated value is in good agreement with the 2 × 12% = 24% value from the dephasing fit. (The factor of 2 arises from the fact that only half of S_0 is due to bridge glycyls, as described above.) The agreement is better than that for the FPBV−PG complex, possibly because the position of the CF_3 of LY309687 makes the dephasing limit less sensitive to bridge conformational variability.

LCTA Complexes with [1-^{13}C]Glycine-Labeled Whole Cells. The $^{13}C\{^{19}F\}$ REDOR dephasing for the complex of LCTA-1049 with whole cells of *S. aureus* grown on media containing [1-^{13}C]glycine and L-[ϵ-^{15}N]lysine is similar to that for the corresponding complex of LCTA-1110 (Figure 8, open circles). The solid lines indicate the calculated dephasing assuming the locations of the ^{19}F relative to the pentaglycyl bridge shown in Figure 9 and a total dephasing after 30 ms of 7.3%. These arrangements provided the best match between calculated and observed dephasing values and placed the ^{19}F of both glycopeptides approximately 6 Å from the nearest glycyl carbonyl carbon and 11 Å from the farthest one, at either end of the helical bridge. The dashed lines show the calculated dephasing when the ^{19}F was moved away from the ends and placed near the middle of the bridge.

The calculated asymptotic dephasing limit for the two LCTA−PG complexes is (0.30)(0.46) = 13%, where the first factor is the binding-site occupancy from the binding assay and the second, the fraction of stems ending in D-Ala-D-Ala. The calculated value is in good agreement with the 2 × 7.3% = 15% value from the dephasing fit. The observed increase in dephasing for evolution times longer than 30 ms in Figure 8 suggests that the ^{19}F of the eremomycin derivatives is within range of a second bridge.

$^{15}N\{^{19}F\}$ REDOR of Glycopeptide−Whole Cell Complexes. The $^{19}F_3$ of LY309687 is positioned near the middle of the pentaglycyl helix but closer to the cross-link than the bridge-

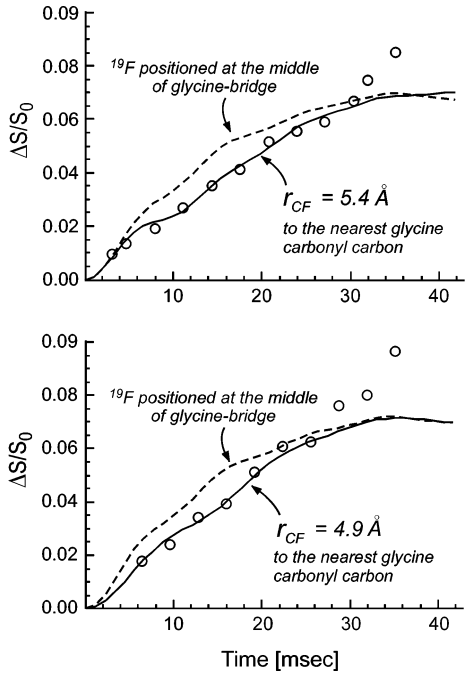

FIGURE 8: $^{13}C\{^{19}F\}$ dephasing ($\Delta S/S_0$) for whole cells of *S. aureus* labeled with [1-^{13}C]glycine and complexed with LCTA-1049 (top) and LCTA-1110 (bottom). The solid line is the calculated dephasing assuming the five $^{13}C-^{19}F$ distances in Figure 9 (top for LCTA-1049 and bottom for LCTA-1110) and a total dephasing of 7.3%. The dashed lines show the calculated dephasing assuming the five $^{13}C-^{19}F$ distances of the LY309687 arrangement in Figure 7 (bottom).

link end of the α-helical bridge, consistent with the absence of an amide peak in the $^{15}N\{^{19}F\}$ REDOR difference spectrum (Figure 10, bottom). This means that the fluorine has an average position that is at least 10 Å from the lysyl nitrogen connecting the bridge to the stem (*14*). The positioning of the fluorine of the FPBV−PG complex (data not shown) is the same as that in the [^{19}F]oritavancin−PG complex (*15*), at the cross-link end of the bridge. The ^{19}F of LCTA-1049, however, is near the bridge-link end of the α-helical bridge, as shown by the presence of an amide peak in the $^{15}N\{^{19}F\}$ REDOR difference spectrum (Figure 10, top). A similar REDOR difference was observed for the LCTA-1110−whole-cell complex. Thus, the fluorines for both LCTA glycopeptides must be close to the lysyl ϵ-nitrogen connecting the pentaglycyl segment to the stem (*5*). The REDOR dephasing shown in Figure 11 indicates a distribution of $^{19}F-^{15}N$ distances centered at 7.9 Å with a width of ±3 Å for both LCTA glycopeptides. The asymptotic dephasing limit of 10% in Figure 11 is close to the 13% calculated value. A summary of the positions of the fluorine labels relative to the bridging pentaglycyl segment for all five glycopeptide−peptidoglycan complexes is shown in Figure 12.

LY309687 Complex with D-*[1-^{13}C]Alanine-Labeled Cell Walls.* The $^{13}C\{^{19}F\}$ REDOR NMR spectra for a complex of LY309687 and cell walls of *S. aureus* grown on media containing D-[1-^{13}C]alanine and a racemase inhibitor are shown in Figure 13. The cell-wall preparation removes the D-Ala esters of all teichoic acids (*31*). Nevertheless, for long evolution times, the full-echo spectrum shows two chemical environments for the D-Ala carbonyl carbon (Figure 13, bottom right). In addition, the center of the carbonyl carbon peak, which is prominent for shorter evolution times,

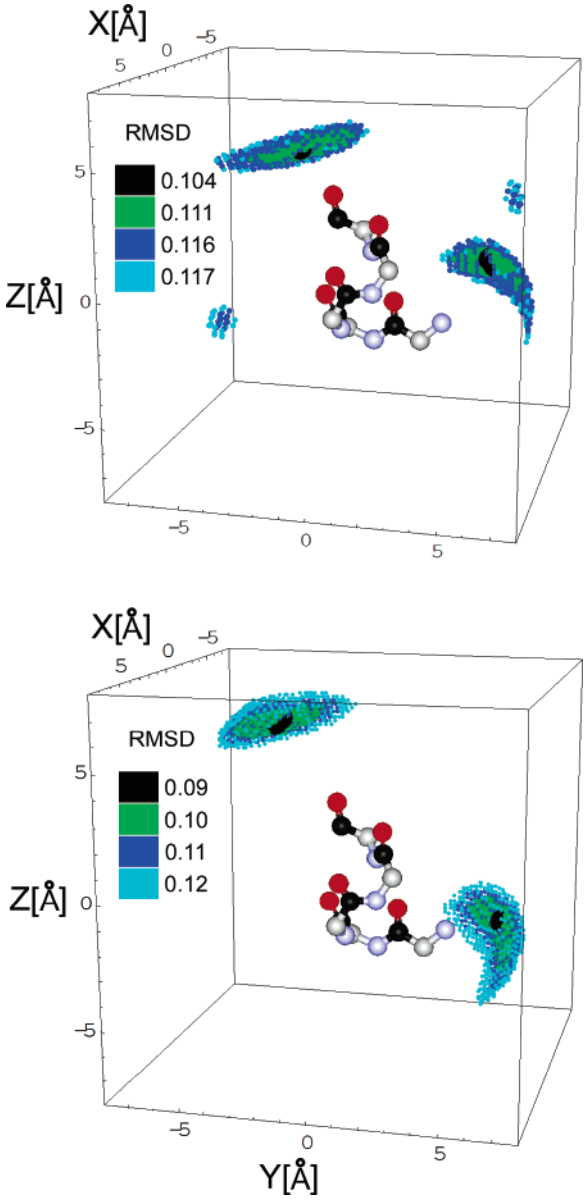

FIGURE 9: Possible positions of fluorine relative to the bridging pentaglycyl helix in peptidoglycan complexes of LCTA-1049 (top) and LCTA-1110 (bottom). The description of the color coding is the same as that in Figure 7.

represents a third environment. Thus, the CF_3 of LY309687 is coupled to three different stem alanines.

We assigned two of these stem alanines to the D-Ala-D-Ala of the binding site (D-Ala-4, 174 ppm; D-Ala-5, 178 ppm) and the third to the single D-Ala of the cross-link site of the neighboring stem (175 ppm). The shift of the D-Ala-4 carbonyl carbon suggests an extended conformation for the stem terminus (*32*), which is in agreement with solution-state ^{13}C NMR assignments for modified glycopeptides (*33*). Previous REDOR experiments on [^{19}F]oritavancin−PG complexes had not detected the D-Ala-D-Ala binding site (*15*). The increased dephasing created by a CF_3 super spin relative to a single fluorine plus the shifted location of the CF_3 away from the cross-link end of the pentaglycyl bridge combine to bring the D-Ala-D-Ala binding site within dephasing range.

The calculated $^{13}C\{^{19}F\}$ REDOR dephasing (solid lines) for three different arrangements of the three D-Ala residues is shown in Figure 14. All three assume a 35% asymptotic

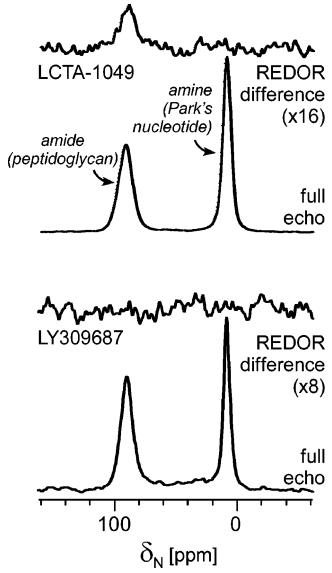

FIGURE 10: $^{15}N\{^{19}F\}$ REDOR spectra of whole cells of *S. aureus* labeled with [ϵ-^{15}N]lysine and complexed with LCTA-1049 (top) and LY309687 (bottom) after dipolar evolution for 96 rotor cycles. The full-echo spectrum (S_0) is at the bottom of the figure, and the REDOR difference ($\Delta S = S_0 - S$, where S is the dephased echo) is shown at the top. The ϵ-^{15}N amide nitrogens of the Gly-5-Lys bridge link appear near 95 ppm. The spectra are the result of the accumulation of 132 000 scans. Magic-angle spinning was at 5000 Hz.

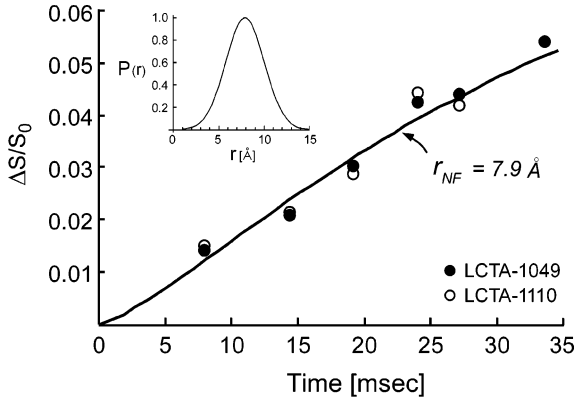

FIGURE 11: $^{15}N\{^{19}F\}$ dephasing ($\Delta S/S_0$) for whole cells of *S. aureus* labeled with [ϵ-^{15}N]lysine and complexed with LCTA-1049 (●) and LCTA-1110 (○). The solid line is the calculated dephasing assuming the distribution of $^{15}N-^{19}F$ distances shown in the inset and a total dephasing of 10%.

dephasing limit, and all three give reasonable fits to the data. The top arrangement has three D-[1-^{13}C]alanines with identical distances of 8.6 Å to the $^{19}F_3$. The middle arrangement has two D-[1-^{13}C]alanines closer to $^{19}F_3$ at 6.0 Å and a third, more distant one at 10 Å. The bottom arrangement has one D-[1-^{13}C]alanine at 8.4 Å and the other two at 11.5 Å. Of the three, only the bottom arrangement is physically plausible. The top and middle are impossible because the lattice distance between the CF_3 of LY309687 and the [1-^{13}C]D-Ala-D-Ala to which it is bound must exceed 10 Å (*29*). The shorter $^{13}C-^{19}F_3$ distance of the bottom arrangement is similar to the observed 8-Å distance between the ^{19}F on the biphenyl of [^{19}F]oritavancin and the D-[1-^{13}C]alanine of the neighboring stem cross-linked to the bridging pentaglycyl segment of the bound stem (Figure 1). The two 11.5-Å distances correspond to the $^{13}C-^{19}F_3$ distances to the D-Ala-D-Ala terminus of the bound stem.

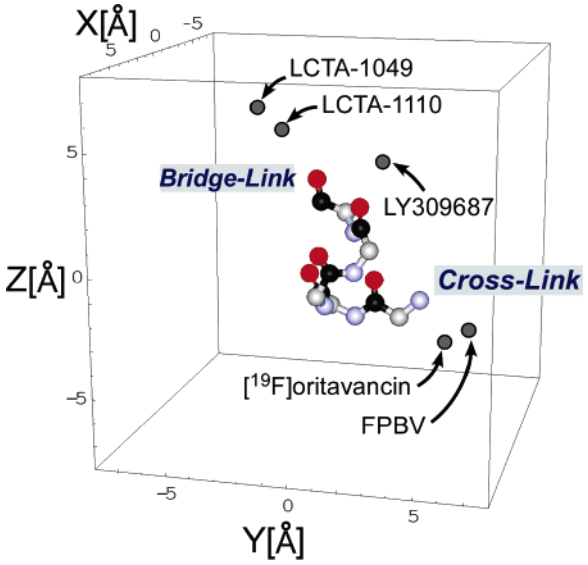

FIGURE 12: Positions of the fluorines of five glycopeptides relative to the bridging pentaglycyl helix in whole-cell *S. aureus* glycopeptide−peptidoglycan complexes. The positions are based on the results shown in Figures 7, 9, and 10 and ref 15.

The calculated asymptotic dephasing limits for Figure 14 are the products of four factors: (i) the fraction of stems that end in D-Ala-D-Ala and that are potential binding sites; (ii) the binding-site occupancy; (iii) the number of D-Ala ^{13}C labels coupled to each CF_3; and (iv) the inverse of the average number of D-Ala residues per peptidoglycan stem. The product of the first three factors is ΔS, and the fourth factor is S_0^{-1}; therefore, the product of all four is $\Delta S/S_0$. The TEDOR experiment mentioned above (*30*) has established that the fraction of D-Ala-D-Ala stems is 0.46, which specifies the average number of D-Ala residues per stem to be 1.49. The binding assay (*15*) measured an occupancy of 35% for LY309687 complexed to cell walls. The bottom model in Figure 14 has three D-alanines coupled to each CF_3. Thus, the calculated asymptotic dephasing limit is (0.46)(0.35)-(3)/(1.49) = 32%. The observed asymptotic dephasing limit is 35%, in agreement with the calculated value. This is true, despite the fact that LY309687 presumably binds to stems that have no pentaglycyl segment attached to the lysyl ϵ-nitrogen at Gly-5 (15% of all stems) (*15*) or to stems that are nonbridging and have no cross-link at Gly-1 (20% of all stems) (*20*), complexes for which the contribution to the dephasing limit would be reduced by one-third.

DISCUSSION

Models for [^{19}F]Oritavancin Complexes. The model of the [^{19}F]oritavancin−PG complex that we will use for structural comparisons resulted from an effort to make the same basic structure satisfy the REDOR data for all five glycopeptide−peptidoglycan complexes. No major structural rearrangements of the starting [^{19}F]oritavancin model (see Materials and Methods) were required to achieve this goal. Nevertheless, substantive differences are present between what we will call the final or modified [^{19}F]oritavancin model (Figures 15 and 16, top) and the MD model (*30*) of Cegelski et al. (Figures 15 and 16, bottom). The differences are as follows: (i) The pentaglycyl bridge in the modified model is helical, consistent with the reported glycyl carbonyl carbon chemical shifts (*15*) and the pentaglycyl end-to-end distance

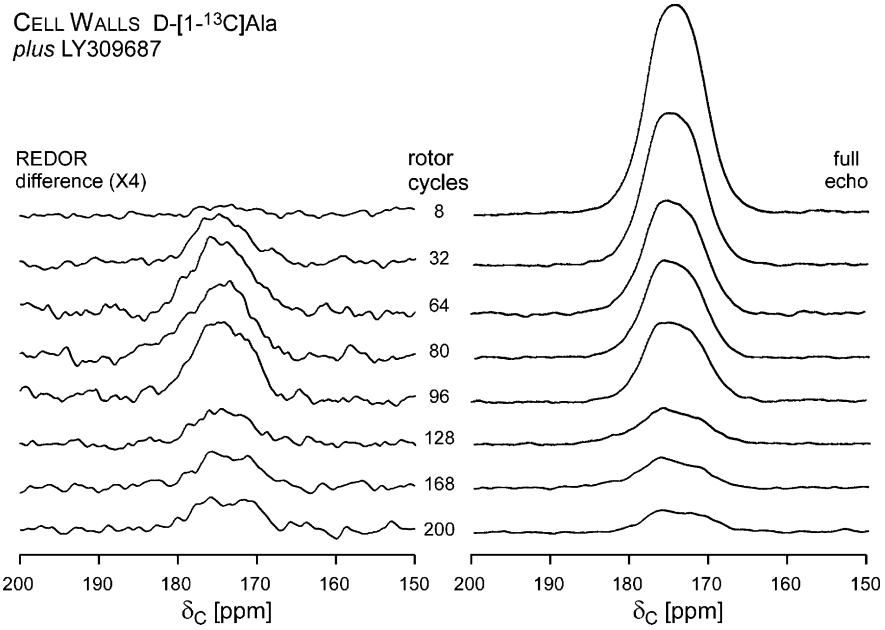

FIGURE 13: $^{13}C\{^{19}F\}$ REDOR spectra of the cell walls of *S. aureus* labeled with D-[1-^{13}C]alanine and complexed with LY309687. The cells were grown in the presence of the alanine racemase inhibitor, alaphosphin. The full-echo spectra (S_0) are at the right of the figure, and the REDOR differences ($\Delta S = S_0 - S$, where S is the dephased echo) are shown at the left. The carbonyl carbons of the D-Ala-D-Ala stem are resolved after 200 rotor cycles of dipolar evolution (bottom right). Each spectrum is the result of the accumulation of 80 000 scans. Magic-angle spinning was at 5000 Hz.

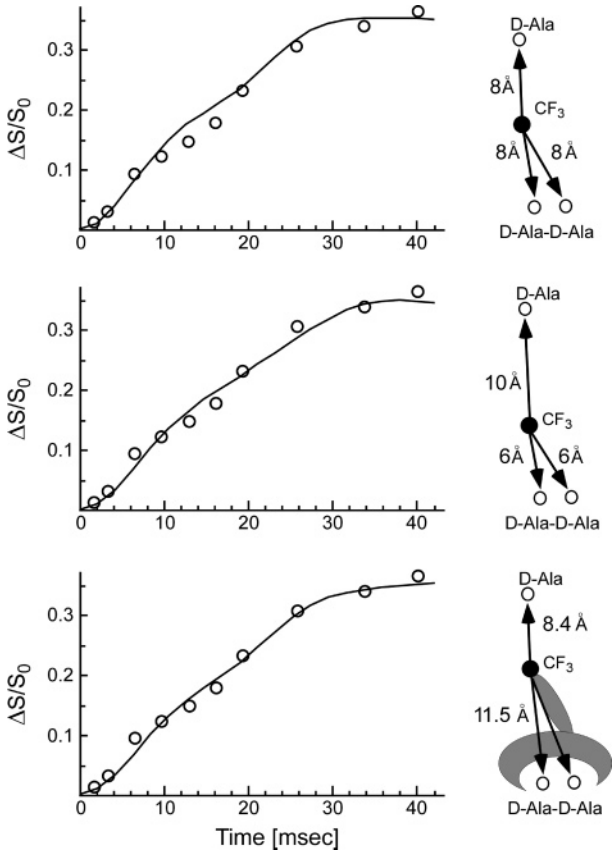

FIGURE 14: $^{13}C\{^{19}F\}$ dephasing ($\Delta S/S_0$) for the spectra in Figure 13. The open circles show the experimental dephasing and the solid lines, the calculated dephasing assuming the distribution of $^{13}C-C^{19}F_3$ distances shown to the right with a total dephasing of 35%.

(*20*). (ii) The pentaglycyl bridging segment is lowered into a protective cleft formed by the 4-epi-vancosamine and the glycopeptide core so that it will be in position to account for the $^{13}C\{^{19}F\}$ and $^{15}N\{^{19}F\}$ dephasing results of the LTCA−PG complexes (Figures 8 and 11). (iii) The D-iso-Gln of the bound stem is moved up toward the 4-epi-vancosamine moiety, and (iv) the unbound neighboring stem is moved away from the *C*-terminus of the glycopeptide core and proximity to the bound stem. In the discussion of other structural modifications that follows, reference to the [^{19}F]-oritavancin−PG model will always be to the modified model of Figures 15 and 16 (top).

4-Epi-Vancosamine. The peptidoglycan complexes of FPBV and [^{19}F]oritavancin are qualitatively similar (Figures 16 and 17, top), which is not surprising because both antibiotics have identical peptidoglycan-binding domains and disaccharide substituents. The difference between the two is the 4-epi-vancosamine of [^{19}F]oritavancin. This sugar is located far from the D-Ala-D-Ala binding pocket of the glycopeptide aglycon and generally is presumed not to participate in dipeptide binding. However, a study of glycopeptide binding to *N*,*N*′-diacetyl-L-Lys-D-Ala-D-Ala (tripeptide) showed that sugars on glycopeptides often improve antimicrobial activities without enhancing binding affinities (*34*). For example, both chloroeremomycin and eremomycin are 5- to 10-fold more active against VSE than vancomycin, despite binding affinities to tripeptide that are 23-fold and 3-fold lower, respectively (*35*, *36*).

The removal of 4-epi-vancosamine from the [^{19}F]oritavancin−PG complex (which results in the FPBV−PG complex) has a measurable effect on the position of the fluorine relative to the pentaglycyl helical bridge (Figure 12). One possible explanation for the shift is that 4-epi-vancosamine helps to bind the bridging pentaglycyl segment and the bound stem. The model of the [^{19}F]oritavancin−PG complex (Figure 16, top) shows 4-epi-vancosamine in proximity to the bridge and bound stem. The pentaglycyl bridge is in the cleft between the epi-vancosamine and the core of the [^{19}F]oritavancin, whereas the D-iso-Gln of the

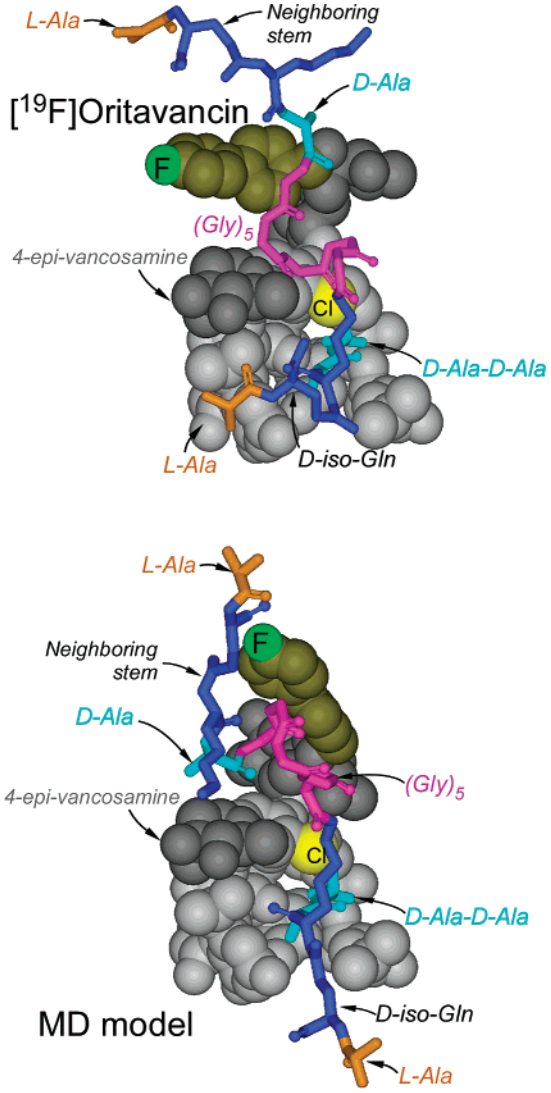

FIGURE 15: Two models of the [^{19}F]oritavancin complex with the peptidoglycan of *S. aureus*. The MD model at the bottom of the Figure is due to Cegelski et al. (*30*) and resulted from a molecular dynamics simulation (with energy minimization) of binding in a peptidoglycan matrix consisting of four glycan chains, each eight repeat units long. The binding was restrained by the REDOR results of refs *15* and *30*. The modified model at the top was constructed by adding an energy-minimized pentaglycyl helix to a stem fragment, D-Ala-D-iso-Gln-L-Lys-D-Ala-D-Ala, bound to [^{19}F]oritavancin. The structure of this complex was based on the crystal structure of Lys-D-Ala-D-Ala bound to chloroeremomycin (*29*). The pentaglycyl helix was positioned to satisfy all relevant REDOR restraints (*15*), including those from Figures 6, 8, 11, and 14. The binding stem and attached pentaglycyl segment (magenta) have been moved proximate to the 4-epi-vancosamine moiety. The pentaglycyl segment of the neighboring stem is unconstrained by any REDOR results and has been omitted.

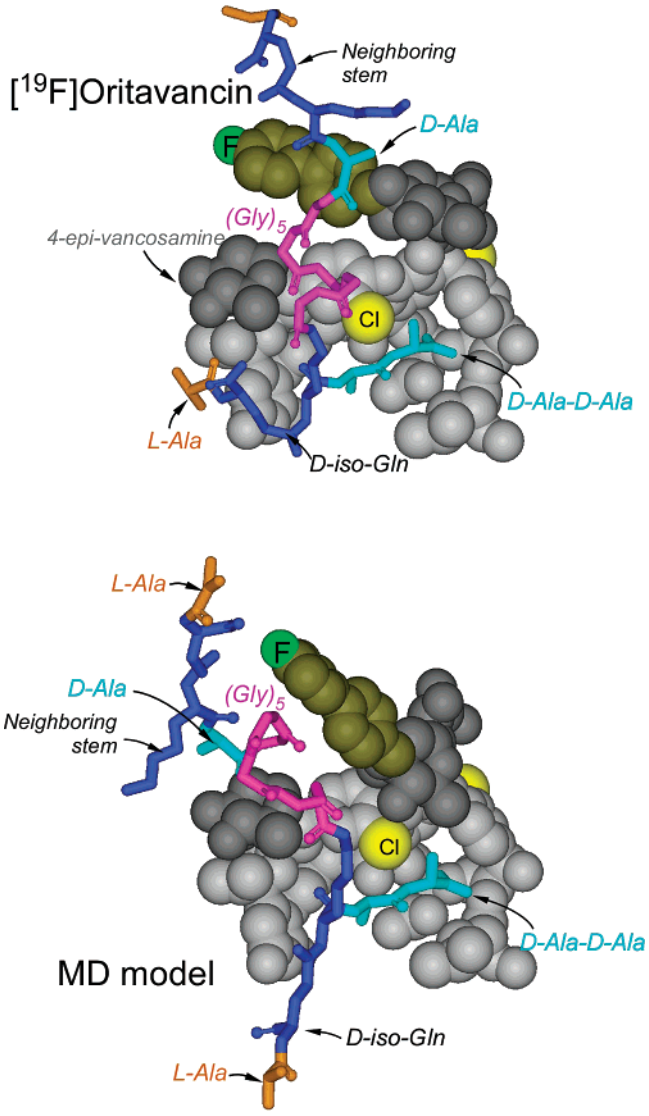

FIGURE 16: Different perspective of the two models in Figure 15.

stem is in the same cleft between the epi-vancosamine and the *C*-terminus of the [^{19}F]oritavancin.

The placement of the bridge near 4-epi-vancosamine is supported by the results of Figures 8 and 11. The placement of the D-iso-Gln near 4-epi-vancosamine is supported by biochemical evidence. Vancomycin-resistant *S. aureus* (Mu50) has reduced amidation of D-iso-Gln (resulting in D-iso-Glx), but the revertants (vancomycin-susceptible) show no sign of reduced amidation (*37*, *35*). Furthermore, vancomycin activity is more strongly antagonized by a pentapeptide stem with D-iso-Glu than by a pentapeptide stem with D-iso-Gln (*38*). This evidence suggests that 4-epi-vancosamine interactions with the pentaglycyl segment of the binding stem and *C*-terminus interactions with the D-iso-Gln of the same stem may be an important part of the improved efficacy of vancomycin analogues against VRE. Glycopeptides with the 4-epi-vancosamine (chloroeremomycin and [^{19}F]oritavancin, for example) are approximately 10-fold more potent against VRE than the corresponding glycopeptides without 4-epi-vancosamine (vancomycin and FPBV, respectively) (*39*).

Modified Disaccharides. To satisfy the ^{13}C{^{19}F} dephasing results of Figure 6 (bottom), the CF_3 group of LY309687 was moved off of the axis of the pentaglycyl helix and placed closer to the middle of the helix (Figure 12). The resulting disaccharide conformation of the LY309687−PG complex (Figure 17, bottom) is clearly different from that of the [^{19}F]-oritavancin−PG complex (Figure 16, top), even though both glycopeptides are active against VRE. It seems unlikely therefore that these glycopeptides act as specific enzyme inhibitors (*10*). We suggest instead that the modified disaccharides enhance the potency of vancomycin analogues by a combination of two effects: (i) improved binding by compensation for weak interactions between the vancomycin aglycon and D-Ala-D-Lac (depsipeptide) terminating pepti-

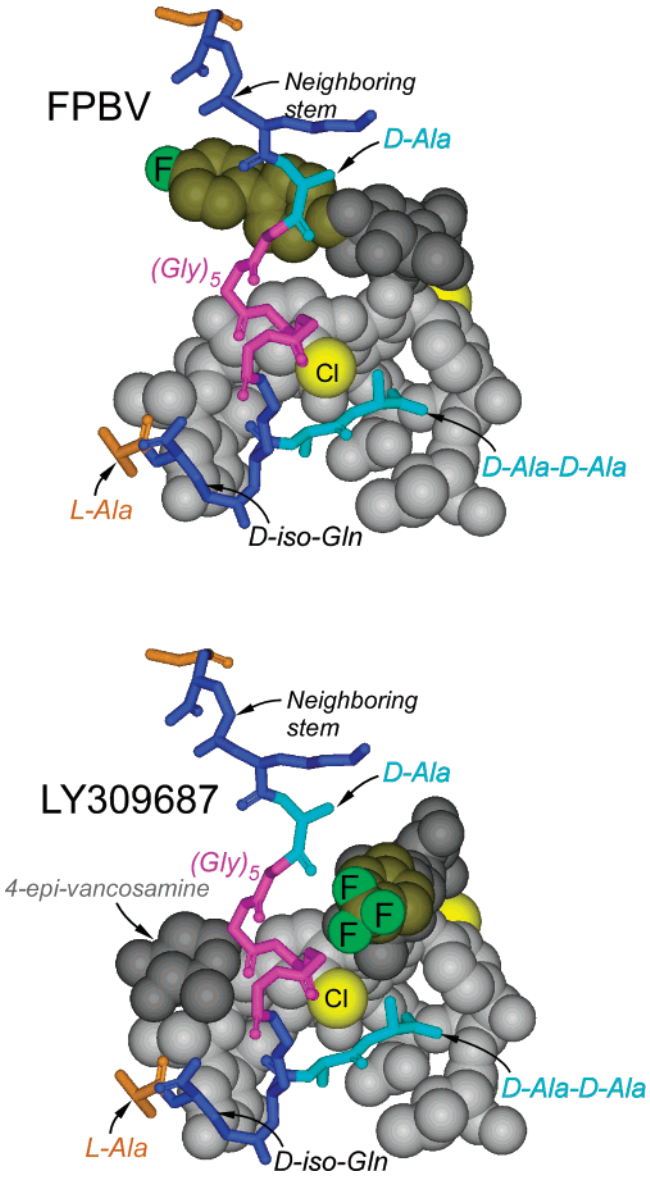

FIGURE 17: Molecular models of peptidoglycan complexes of FPBV (top) and LY309687 (bottom). The perspective is the same as that shown for the [^{19}F]oritavancin complex in Figure 16 (top). The positioning of the CF_3 group of LY309687 to satisfy the REDOR results of Figure 6 (bottom) moves the disaccharide moiety of the glycopeptide away from the connection to the neighboring stem.

doglycan precursors and (ii) direct inhibition of normal peptidoglycan biosynthesis by a mechanism that depends on the steric bulk of the disaccharide substituent.

This proposal is based on two sets of observations. First, even though the lengths of the hydrophobic substituents are important, a range of length and bulk results in about the same activity for semisynthetic vancomycins (*39*). Figure 3 shows a series of chloroeremomycin derivatives with varying lengths of aliphatic chains attached at the disaccharide position. The MICs of these modified compounds against VRE and VSE are plotted as a function of the hydrophobic chain length (measured by the number of C−C bonds). As the hydrophobic chains are lengthened, the drug potency initially improves. An optimal length is near the center of a broad MIC minimum between 11 and 14 C−C bonds, with a 1000-fold increase in antimicrobial activities against VRE relative to that of vancomycin.

LY309687 falls into a second category of chloroeremomycin derivatives, with a hydrophobic chain length of 7 C−C bonds. This category exhibits an approximately 100-fold increase in antimicrobial activity against VRE. We believe that long chains are needed for steric bulk to interfere with transpeptidation or transglycosylation (*15*), but chains that are too long may have difficulty undergoing conformational rearrangements and may be inappropriately positioned to have any effect on biosynthesis once they have reached the membrane.

The second set of observations supporting a dual role for the disaccharide moiety is that the derivative of chloroeremomycin with the longest hydrophobic chain in Figure 3 had the same level of antimicrobial activity in in vitro assays against both VSE and VRE strains, whereas the level of antimicrobial activity of the chloroeremomycin parent compound against VRE decreased by more than an order of magnitude (*39*, *40*). The modified disaccharide of the long-chain chloroeremomycin derivative, therefore, appears to stabilize the weak binding between the glycopeptide and D-Ala-D-Lac terminated peptidoglycan precursors of VRE (presumably by multivalent sugar interactions with either glycan chains or peptide stems), in addition to interfering with peptidoglycan biosynthesis.

C-Terminus Modified Eremomycin. Models of the peptidoglycan complexes of LCTA-1049 and LCTA-1110 (Figure 18) show three differences from the corresponding models of [^{19}F]oritavancin, FPBV, and LY309687: (i) the eremomycin derivatives are missing chlorine at the sixth amino acid of the aglycon; (ii) the ^{19}F labels are positioned at the bridge-link of the bound peptidoglycan; and (iii) the L-Ala-D-iso-Gln of the binding stem is repositioned to accommodate the hydrophobic moiety at the aglycon *C*-terminus.

The chlorine missing from eremomycin alters the D-Ala-D-Ala binding pocket and affects binding to the tripeptide Acyl-L-Lys-D-Ala-D-Ala. For example, the binding affinity of eremomycin to tripeptide is 26-fold less than that of chloroeremomycin (*40*). Nevertheless, despite the lower binding affinity, the antimicrobial activity of eremomycin is almost the same as that of chloroeremomycin and 5- to 10-fold greater than that of vancomycin. We believe that these activities are not related to the missing chlorine but are the result of the 4-epi-vancosamine interactions described above.

The ^{19}F of the LCTA glycopeptides are positioned at the bridge-link of the bound peptidoglycan as required by ^{13}C-{^{19}F} and ^{15}N{^{19}F} dephasing (Figures 8 and 11). Although the LCTAs and the disaccharide-modified glycopeptides have similar hydrophobic substituents, in the cell-wall complexes, the substituents are positioned at opposite ends of the bridging pentaglycyl segments (Figures 17 and 18). Nevertheless, a series of alkylaminomethylated derivatives of eremomycin (*41*) and teicoplanin aglycon (*42*) with a hydrophobic substituent at the 7d-position of the resorcinol ring at amino acid 7 showed a hydrophobic substituent-length dependence of activity similar to that of the disaccharide-modified chloroeremomycin derivatives of Figure 3. Significant activity against VRE was observed for both N′-substituted derivatives of eremomycin (*41*) and teicoplanin aglycon (*42*) with the hydrophobic moiety, $NHC_{10}H_{21}$, positioned near the *C*-terminus.

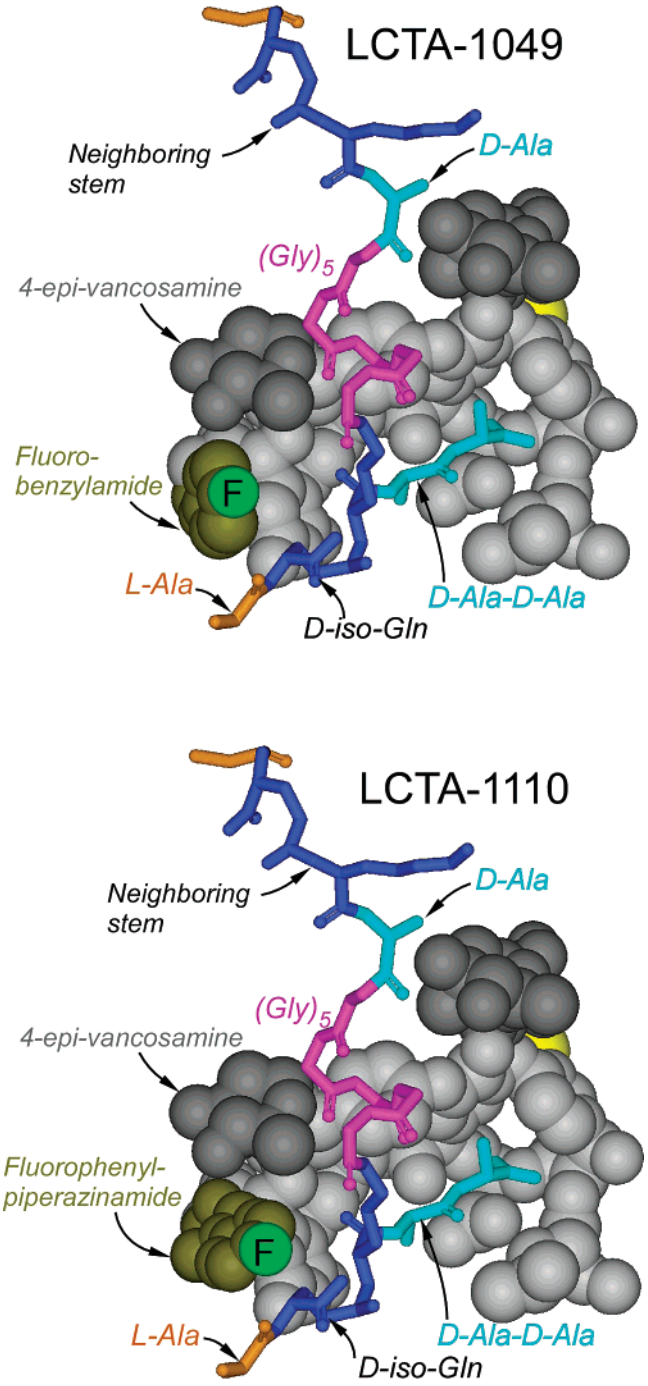

FIGURE 18: Molecular models of peptidoglycan complexes of LCTA-1049 (top) and LCTA-1110 (bottom). The D-Ala-D-iso-Gln residues of the bound pentapeptide stem has been moved away from the 4-epi-vancosamine for both of these bound glycopeptides relative to their positions for the corresponding complexes of FPBV and LY309687 in Figure 17.

For the most part, however, the *C*-terminus and disaccharide-modified glycopeptides have different patterns of antimicrobial activities. For example, LCTA-1049 and LCTA-1110 show little improved activity against VSE relative to eremomycin but a 4-fold improvement against VRE (Table 1). FPBV, however, is more active than its vancomycin parent against both VSE and VRE. In addition, Edman degradation of *C*-terminus-modified eremomycin does not affect its antimicrobial activity. For example, 4-[(4-chlorophenyl)benzyl]amide of eremomycin and 4-[(4-chlorophenyl)benzyl]amide of des(*N*-methylleucyl)eremomycin have identical activities against VRE with an MIC range of 2−4 μg/mL (*43*). This is in contrast to the disaccharide-modified *N*′-[*p*-(*p*-chlorophenyl)benzyl]vancomycin (CPBV), for which Edman degradation results in significant loss in activity. Thus, the MIC of CPBV against VRE (*E. faecium*) is 16 μg/mL, whereas that of des(*N*-methylleucyl)CPBV is 40−80 μg/mL (*10*).

All of these observations suggest that when disaccharide hydrophobic moieties are at the *C*-terminus, as they are for the LCTA glycopeptides, their role is exclusively to stabilize the weak drug interaction with depsipeptide-terminated peptidoglycan. When the moieties are attached to the disaccharides, then they function both to stabilize and to interfere directly with peptidoglycan biosynthesis. In the next three sections, we will discuss a mode of action for vancomycin, eremomycin, and chloroeremomycin and their derivatives that interprets known structure−activity relationships in terms of the models shown in Figures 16−18.

Glycopeptide−Peptidoglycan Complexes in the Mature Cell Wall as Models for Complexes at the Membrane Interface. There are three types of glycopeptide binding sites in whole cells of *S. aureus*. Glycopeptide binds to the D-Ala-D-Ala termini of (i) mature peptidoglycan, (ii) nascent peptidoglycan, and (iii) lipid II. Mature peptidoglycan is localized in the cell wall, disassociated from the bacterial membrane, and distinguished by about 60% cross-linking (*3*). Nascent peptidoglycan (incompletely formed with few cross-linked chains) and lipid II (peptidoglycan monomer) are proximate and possibly still tethered to the membrane. Only glycopeptide binding to nascent peptidoglycan and lipid II will result in inhibition of peptidoglycan biosynthesis. The mature peptidoglycan competes for glycopeptide binding and restricts access to the bacterial membrane, thereby reducing the effectiveness of the glycopeptide. In fact, preferential binding of glycopeptide in a thickened mature cell wall (with reduced cross-linking) is one of the mechanisms of vancomycin resistance in *S. aureus* (*34*).

The models shown in Figures 16−18 have been developed for glycopeptide complexes with mature cell walls. However, these peptidoglycan complexes are not in the most heavily cross-linked regions of the cell wall because D-Ala-D-Ala stem termini are, for the most part, missing from such regions (*30*). Rather, the complexes are in partially cross-linked regions, where isolated D-Ala-D-Ala stems are likely. The complex consists of an aglycon binding site, a bound stem, its attached pentaglycyl segment, the cross-link, and the neighboring stem of an adjacent glycan chain. The presence of all of these components has been established by experimental REDOR restraints between the glycopeptide and the pentaglycyl bridge (Figures 6 and 8), bridge-link (Figure 10), cross-link (Figure 5 in ref *30*), D-Ala-D-Ala bound-stem terminus (Figure 14), and L-Ala neighboring-stem base (Figure 3 in ref *44*). This combination is what we will use to describe the active site of the enzyme at the membrane surface (with the exception that the cross-link has not been formed yet). No drug dimers will be included in the complexes because their bulk and geometry are not consistent with the local ordering of growing chains at the membrane surface, which will be the key to the proposed drug mode of action.

Mode of Action. Proteins at the bacterial membrane carry out the final steps in peptidoglycan biosynthesis: transgly-

cosylation and transpeptidation. Transglycosylation is the extension of the nascent peptidoglycan polymer by the incorporation of the lipid II monomer. Transpeptidation is the cross-linking of nascent peptidoglycan to surrounding neighboring glycan chains, thereby forming a 3D mesh. Transglycosylation and transpeptidation must be tightly coupled (*46*, *47*) to allow *S. aureus* to reach average cell-wall cross-linking levels of 60% (*30*). If the transglycosylation and transpeptidation were uncoupled, then such massive cross-linking of the fully extended peptidoglycan chains of the immature cell wall would be impossible because of chain entanglements in a partially cross-linked matrix (*48*).

The glycan chains of the cell-wall peptidoglycan are helical (*45*), and the pentapeptide stems that extend from successive glycan repeat units differ in orientation with respect to the helix axis (*45*). Thus, it seems reasonable to suppose that a glycan chain must be initiated with a nearest-neighbor chain as a template to ensure the correct orientation of stems that are to be cross-linked. The notion of a template in the production of cell-wall peptidoglycan has been proposed before. Höltje has suggested that in *E. coli* a replicase holoenzyme attaches to a docking or template glycan strand and synthesizes three new strands that are cross-linked as the enzyme slides along the template (*49*). In this scheme, the bottom-most newly synthesized strand is not fully cross-linked and serves as the template for the next peptidoglycan layer. The experimental evidence supporting this mechanism is based on the failure of cell-wall-free (and hence template-free) spheroplasts and protoplasts to reform cell walls of the proper shape (*50*, *51*).

We propose that binding of the disaccharide-substituted glycopeptides shown in Figures 16 and 17 to the D-Ala-D-Ala terminus of a stem at the membrane interface interferes with the biosynthesis of a neighboring chain and not the glycan chain to which the drug is bound. We assume that the active site for transglycosylation includes the start of a nascent peptidoglycan chain, the lipid II monomer to extend this new chain, and the pentapeptide stem (or the pentaglycyl segment of that stem) from the nearest-neighbor glycan chain acting as a template. We believe that a disaccharide-substituted glycopeptide binds to the stem and attached pentaglycyl fragment of a template strand within the peptidoglycan matrix so that the growth of the nearest-neighbor glycan chain is either blocked (inhibition of transglycosylation) or occurs with adjacent stems misaligned and disordered (inhibition of cross-linking). In effect, these vancomycin-like glycopeptides kill by interfering with template recognition during peptidoglycan biosynthesis. Such drugs are also capable of sequestering lipid II (with D-Ala-D-Ala stem termini) and directly inhibiting transglycosylation.

In terms of the models shown in Figures 16 and 17, we consider the bound D-Ala-D-Ala terminus as part of the signaling stem of the template strand. The sugars of the neighboring stem are then the starting point for a new glycan strand. The alteration of the binding site for a D-Ala-D-Lac stem terminus and the likely resulting conformational rearrangement of the less tightly bound stem can be compensated by the protection offered to the pentaglycyl segment of the bound stem by the 4-epi-vancosamine substituent and by the positioning of the disaccharide moiety. We propose that these groups form a secondary binding site for pentaglycyl segments of the effective VRE-killing [^{19}F]oritavancin and

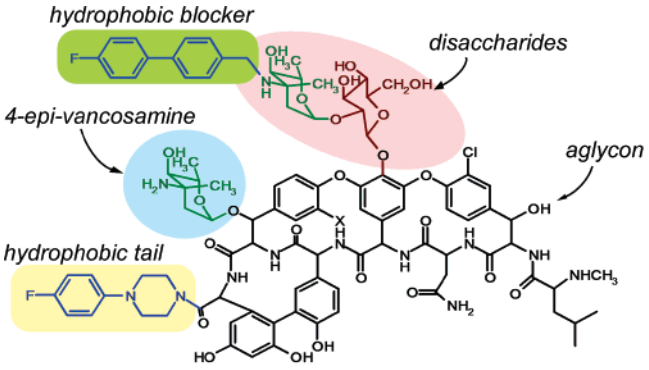

FIGURE 19: Composite structure of a generalized eremomycin-type antibiotic showing the five proposed functional moieties responsible for antimicrobial activity. X = Cl (Chloroeremomycin) and X = H (eremomycin).

FPBV shown in Figures 16 (top) and 17 (top). LY309687, shown in Figure 17 (bottom), has reduced activity relative to that of [^{19}F]oritavancin because of the shift in position of its disaccharide away from the neighboring stem and the site of new-chain biosynthesis.

The LCTA eremomycin analogues (Figure 18), in contrast, are apparently effective against VRE, not by increasing the size of the steric blocker interfering with chain growth and cross-linking but rather by retaining the position of its disaccharide moiety in peptidoglycan complexes binding with stems with a D-Ala-D-Lac terminus. We believe that this is accomplished through attractive nonbonded interactions of the hydrophobic moiety of the drug and the L-Ala-D-iso-Gln component of the bound stem. These drugs may then operate similarly to vancomycin, binding to and sequestering lipid II thereby inhibiting transglycosylation (*3*).

Anatomy of Vancomycin-Like Glycopeptides. We summarize the preceding discussion of the REDOR-based models of [^{19}F]oritavancin, FPBV, and LY309687−PG complexes and suggestions correlating glycopeptide structure and function (and proposed mode of action) by dividing the structure of vancomycin, eremomycin, and chloroeremomycin derivatives into five parts (Figure 19). The first part is the aglycon, which is well established as a D-Ala-D-Ala binding domain. This part is essential for binding to nascent peptidoglycan and lipid II at the membrane surface. The second part is the disaccharide (glucose-vancosamine) attached at the fourth amino acid position of the aglycon. The disaccharide helps stabilize complexes with depsipeptide-terminated stems. The disaccharide also acts as a scaffold for the attachment of a hydrophobic blocker, and the disaccharide conformation is important for the placement of the blocker. The hydrophobic blocker (typically an alkyl side chain) is itself the third part of the structure. The hydrophobic blockers are positioned to interfere with a function of transglycosylase or transpeptidase, possibly the registration or ordering of stems of lipid II relative to those of the adjacent template peptidoglycan chain. The fourth part is the 4-epi-vancosamine, which helps stabilize a bound stem and its attached bridging pentaglycyl segment. The fifth part is a hydrophobic tail located at the *C*-terminus of the glycopeptide; the tail also helps stabilize complexes with depsipeptide-terminated peptidoglycan stems. However, when two bulky hydrophobic groups are introduced on eremomycin-type of glycopeptides, the bi-substitu-

tion reduces activity (*52*, *53*). Hence, the generalized bi-substituted eremomycin-type glycopeptide shown in Figure 19 is likely to be less active than a glycopeptide with a single hydrophobic substituent at either the *C*-terminus or the disaccharide positions.

These five parts define the glycopeptide components of a binding site complex. For some glycopeptides, the active binding site may be more complicated than that suggested by Figures 16−18. It is unlikely to be any simpler. The metabolic effects of glycopeptide binding may vary from one drug to another and include the inhibition of transglycosylase, transpeptidase, or both. Additional labeling and solid-state NMR experiments on cell-wall and whole-cell complexes formed under a variety of growth conditions may ultimately help to build a more detailed molecular model and mode of action for vancomycin-like glycopeptides.

ACKNOWLEDGMENT

We thank Ms. Svetlana E. Solovieva and Ms. Elena P. Mirchink, D.Sc., (Gause Institute of New Antibiotics, Moscow) for the syntheses and study of the antibacterial activity of LCTA compounds and Dr. Richard C. Thompson and Dr. Thalia I. Nicas (Lilly Research Laboratories, Indianapolis, IN) for the gift of [^{19}F]oritavancin and LY309687.

REFERENCES

1. Hiramatsu, K., Cui, L., Kuroda, M., and Ito, T. (2001) The emergence and evolution of methicillin-resistant Staphylococcus aureus, *Trends Microbiol. 9*, 486-93.
2. Reynolds, P. (1961) Studies on the mode of action of vancomycin, *Biochim. Biophys. Acta 52*, 403.
3. Cegelski, L., Kim, S. J., Hing, A. W., Studelska, D. R., O'Connor, R. D., Mehta, A. K., and Schaefer, J. (2002) Rotational-echo double resonance characterization of the effects of vancomycin on cell wall synthesis in Staphylococcus aureus, *Biochemistry 41*, 13053−13058.
4. Matsuhashi, S., and Strominger, J. L. (1967) Isolation of thymidine diphosphate D-glucose, thymidine diphosphate D-galactose, and thymidine diphosphate 4-acetamido-4, 6-dideoxy-D-galactose from Pasteurella pseudotuberculosis, *J. Bacteriol. 93*, 2017−2019.
5. Bartley, J. (2002) First case of VRSA identified in Michigan, *Infect. Control. Hosp. Epidemiol. 23*, 480.
6. Clark, N. C., Weigel, L. M., Patel, J. B., and Tenover, F. C. (2005) Comparison of Tn1546-like elements in vancomycin-resistant Staphylococcus aureus isolates from Michigan and Pennsylvania, *Antimicrob. Agents Chemother. 49*, 470−472.
7. Bugg, T. D., Wright, G. D., Dutka-Malen, S., Arthur, M., Courvalin, P., and Walsh, C. T. (1991) Molecular basis for vancomycin resistance in Enterococcus faecium BM4147: biosynthesis of a depsipeptide peptidoglycan precursor by vancomycin resistance proteins VanH and VanA, *Biochemistry 30*, 10408−10415.
8. Arthur, M., Molinas, C., Bugg, T. D., Wright, G. D., Walsh, C. T., and Courvalin, P. (1992) Evidence for in vivo incorporation of D-lactate into peptidoglycan precursors of vancomycin-resistant enterococci, *Antimicrob. Agents Chemother. 36*, 867−869.
9. Malabarba, A., Nicas, T. I., and Thompson, R. C. (1997) Structural modifications of glycopeptide antibiotics, *Med. Res. Rev. 17*, 69−137.
10. Ge, M., Chen, Z., Onishi, H. R., Kohler, J., Silver, L. L., Kerns, R., Fukuzawa, S., Thompson, C., and Kahne, D. (1999) Vancomycin derivatives that inhibit peptidoglycan biosynthesis without binding D-Ala-D-Ala, *Science 284*, 507−511.
11. Goldman, R. C., Baizman, E. R., Longley, C. B., and Branstrom, A. A. (2000) Chlorobiphenyl-desleucyl-vancomycin inhibits the transglycosylation process required for peptidoglycan synthesis in bacteria in the absence of dipeptide binding, *FEMS Microbiol. Lett. 183*, 209−214.
12. Nicas, T. I., Mullen, D. L., Flokowitsch, J. E., Preston, D. A., Snyder, N. J., Zweifel, M. J., Wilkie, S. C., Rodriguez, M. J., Thompson, R. C., and Cooper, R. D. (1996) Semisynthetic glycopeptide antibiotics derived from LY264826 active against vancomycin-resistant enterococci, *Antimicrob. Agents Chemother. 40*, 2194−2199.
13. Rodriguez, M. J., Snyder, N. J., Zweifel, M. J., Wilkie, S. C., Stack, D. R., Cooper, D. G., Nicas, T. I., Mullen, D. L., Butler, T. F., and Thompson, C. R. (1998) Novel Glycopeptide Antibiotics: N-Alkylated derivatives active against vancomycin-resistant enterococci, *J. Antibiot. 51*, 560−569.
14. Gullion, T., and Schaefer, J. (1989) Detection of weak heteronuclear dipolar coupling by rotational-echo double-resonance nuclear magnetic resonance, *Adv. Magn. Reson. 13*, 57−83.
15. Kim, S. J., Cegelski, L., Studelska, D. R., O'Connor, R. D., Mehta, A. K., and Schaefer, J. (2002) Rotational-echo double resonance characterization of vancomycin binding sites in *Staphylococcus aureus*, *Biochemistry 41*, 6967−6977.
16. Zhang, T. Y., and Allen, M. J. (1999) An easily prepared, air and moisture stable, resin-bound palladium catalyst for Suzuki cross-coupling reactions, *Tetrahedron Lett. 40*, 5813−5816.
17. Nagarajan, R., Schabel, A. A., Occolowitz, J. L., Counter, F. T., Ott, J. L., and Felty-Duckworth, A. M. (1989) Synthesis and antibacterial evaluation of N-alkyl vancomycins, *J. Antibiot. 42*, 63−72.
18. Miroshnikova, O. V., Printsevskaya, S. S., Olsufyeva, E. N., Pavlov, A. Y., Nilius, A., Hensey-Rudloff, D., and Preobrazhenskaya, M. N. (2000) Structure-activity relationships in the series of eremomycin carboxamides, *J. Antibiot. 53*, 286−293.
19. Printsevskaya, S. S., Solovieva, S. E., Olsufyeva, E. N., Mirchink, E. P., Isakova, E. B., De Clercq, E., Balzarini, J., and Preobrazhenskaya, M. N. (2005) Structure−activity relationship studies of a series of antiviral and antibacterial aglycon derivatives of the glycopeptide antibiotics vancomycin, eremomycin, and dechloroeremomycin, *J. Med. Chem. 48*, 3885−3890.
20. Tong, G., Pan, Y., Dong, H., Pryor, R., Wilson, G. E., and Schaefer, J. (1997) Structure and dynamics of pentaglycyl bridges in the cell walls of *Staphylococcus aureus* by 13C-15N REDOR NMR, *Biochemistry 36*, 9859−9866.
21. Schaefer, J., and McKay, R. A. (1999) Multi-tuned single coil transmission line probe for nuclear magnetic resonance spectrometer, U.S. Patent 5,861,748.
22. Gullion, T., Baker, D. B., and Conradi, M. S. (1990) New, compensated Carr-Purcell sequences, *J. Magn. Reson. 89*, 479−484.
23. Hing, A. W., Tjandra, N., Cottam, P. F., Schaefer, J., and Ho, C. (1994) An investigation of the ligand-binding site of the glutamine-binding protein of *Escherichia coli* using rotational-echo double-resonance NMR, *Biochemistry 33*, 8651−8661.
24. Weldeghiorghis, T. K., and Schaefer, J. (2003) Compensating for pulse imperfections in REDOR, *J. Magn. Reson. 165*, 230−236.
25. Mueller, K. T., Jarvie, T. P., Aurentz, D. J., and Roberts, B. W. (1995) The REDOR transform: direct calculation of internuclear couplings from dipolar-dephasing NMR data, *Chem. Phys. Lett. 242*, 535−542.
26. de la Caillerie, J.-B. D. E., and Fretigny, C. (1998) Analysis of the REDOR signal and inversion, *J. Magn. Reson. 133*, 273−280.
27. Goetz, J. M., and Schaefer, J. (1997) REDOR dephasing by multiple spins in the presence of molecular motion, *J. Magn. Reson. 127*, 147−154.
28. O'Connor, R. D., and Schaefer, J. (2002) Relative CSA-dipolar orientation from REDOR sidebands, *J. Magn. Reson. 154*, 46−52.
29. Nitanai, Y., Kakoi, K., and Aoki, K. (2000), Protein Data Bank.
30. Cegelski, L., Stueber, D., Mehta, A. K., Kulp, D. W., Axelsen, P. H., and Schaefer, J. (2006) Conformational and quantitative characterization of oritavancin-peptidoglycan complexes in whole cells of *S. aureus* by in vivo ^{13}C and ^{15}N labeling, *J. Mol. Biol. 357*, 1253−1262.
31. Sprott, G., Koval, S., and Schnaitman, C. (1994) in *Methods for General and Molecular Bacteriology* (Gerhardt, P., Murray, R., Wood, W., and Krieg, N., Eds.) pp 72−103, American Society for Microbiology, Washington, DC.
32. Saitô, H. (1986) Conformation-dependent carbon-13 chemical shifts: a new means of conformational characterization as obtained by high-resolution solid-state carbon-13 NMR, *Magn. Reson. Chem. 24*, 835−852.
33. Feher, K., Pristovsek, P., Szilagyi, L., Ljevakovic, D., and Tomasic, J. (2003) Modified glycopeptides related to cell wall peptidoglycan: conformational studies by NMR and molecular modelling, *Bioorg. Med. Chem. 11*, 3133−3140.

34. Vollmerhaus, P. J., Breukink, E., and Heck, A. J. (2003) Getting closer to the real bacterial cell wall target: biomolecular interactions of water-soluble lipid II with glycopeptide antibiotics, *Chem.—Eur. J. 9*, 1556−1565.
35. Cooper, D. G., Snyder, N. J., Zweifel, M. J., Staszak, M. A., Wilkie, S. C., Nicas, T. I., Mullen, D. L., Butler, T. F., Rodriguez, M. J., Huff, B. E., and Thompson, C. R. (1996) Reductive alkylation of glycopeptide antibiotics: synthesis and antibacterial activity, *J. Antibiot. 49*, 575−581.
36. Allen, N. E., LeTourneau, D. L., and Hobbs, J. N., Jr. (1997) Molecular interactions of a semisynthetic glycopeptide antibiotic with D-alanyl-D-alanine and D-alanyl-D-lactate residues, *Antimicrob. Agents Chemother. 41*, 66−71.
37. Boyle-Vavra, S., Labischinski, H., Ebert, C. C., Ehlert, K., and Daum, R. S. (2001) A spectrum of changes occurs in peptidoglycan composition of glycopeptide-intermediate clinical Staphylococcus aureus isolates, *Antimicrob. Agents Chemother. 45*, 280−287.
38. Hanaki, H., Labischinski, H., Inaba, Y., Kondo, N., Murakami, H., and Hiramatsu, K. (1998) Increase in glutamine-non-amidated muropeptides in the peptidoglycan of vancomycin-resistant *Staphylococcus aureus* strain Mu50, *J. Antimicrob. Chemother. 42*, 315−320.
39. Allen, N. E., LeTourneau, D. L., and Hobbs, J. N., Jr. (1997) The role of hydrophobic side chains as determinants of antibacterial activity of semisynthetic glycopeptide antibiotics, *J. Antibiot. 50*, 677−684.
40. Mackay, J. P., Daniel, U., Beauregard, D. A., Maplestone, R. A., and Williams, D. H. (1994) Dissection of the contribution toward dimerization of glycopeptide antibiotics, *J. Am. Chem. Soc. 116*, 4573−4580.
41. Pavlov, A. Y., Lazhko, E. I., and Preobrazhenskaya, M. N. (1997) A new type of chemical modification of glycopeptides antibiotics: aminomethylated derivatives of eremomycin and their antibacterial activity, *J. Antibiot. 50*, 509−513.
42. Pavlov, A. Y., Preobrazhenskaya, M. N., Malabarba, A., Ciabatti, R., and Colombo, L. (1998) Mono and double modified teicoplanin aglycon derivatives on the amino acid no. 7; structure-activity relationship, *J. Antibiot. 51*, 73−78.
43. Printsevskaya, S. S., Pavlov, A. Y., Olsufyeva, E. N., Mirchink, E. P., Isakova, E. B., Reznikova, M. I., Goldman, R. C., Branstrom, A. A., Baizman, E. R., Longley, C. B., Sztaricskai, F., Batta, G., and Preobrazhenskaya, M. N. (2002) Synthesis and mode of action of hydrophobic derivatives of the glycopeptide antibiotic eremomycin and des-(*N*-methyl-D-leucyl)eremomycin against glycopeptide-sensitive and -resistant bacteria, *J. Med. Chem. 45*, 1340−1347.
44. Mehta, A. K., Cegelski, L., O'Connor, R. D., and Schaefer, J. (2003) REDOR with a relative full-echo reference, *J. Magn. Reson. 163*, 182−187.
45. Seligman, S. J., and Pincus, M. R. (1987) A model for the three-dimensional structure of peptidoglycan in staphylococci, *J. Theor. Biol. 124*, 275−292.
46. van Heijenoort, J. (2001) Recent advances in the formation of the bacterial peptidoglycan monomer unit, *Nat. Prod. Rep. 18*, 503−519.
47. Boneca, I. G., Huang, Z. H., Gage, D. A., and Tomasz, A. (2000) Characterization of *Staphylococcus aureus* cell wall glycan strands, evidence for a new beta-*N*-acetylglucosaminidase activity, *J. Biol. Chem. 275*, 9910−9918.
48. Flory, P. J. (1953) *Principles of Polymer Chemistry*, p 388, Cornell University Press, Ithaca, NY.
49. Höltje, J.-V. (1998) Growth of the stress-bearing and shape-maintaining murein sacculus of *Escherichia coli*, *Microbiol. Mol. Biol. Rev. 62*, 181−203.
50. Ghuysen, J. M. (1968) Use of bacteriolytic enzymes in determination of wall structure and their role in cell metabolism, *Bacteriol. Rev. 32*, 425−464.
51. Schwarz, U., Leutgeb, W. (1971) Morphogenetic aspects of murein structure and biosynthesis, *J. Bacteriol. 106*, 588−595.
52. Pavlov, A. Y., Miroshnikova, O. V., Printsevskaya, S. S., Olsufyeva, E. N., Preobrazhenskaya, M. N., Goldman, R. C., Branstrom, A. A., Baizman, E. R., and Longley, C. B. (2001) Synthesis of hydrophobic N′-mono and N′, N″-double alkylated eremomycins inhibiting the transglycosylation stage of bacterial cell wall biosynthesis, *J. Antibiot. 54*, 455−459.
53. Zweifel, M. J., Snyder, N. J., Cooper, R. D., Nicas, T. I., Mullen, D. L., Butler, T. F., and Rodriguez, M. J. (2003) Glycopeptide carboxamides active against vancomycin-resistant enterococci, *J. Antibiot. 56*, 289−295.

BI052660S